Research in the Mathematical Sciences

RESEARCH

Saddle point braids of braided fibrations and pseudo-fibrations

Benjamin Bode[2,1*] and Mikami Hirasawa[3]

*Correspondence:
benjamin.bode@upm.es
[1]Instituto de Ciencias Matemáticas (ICMAT), Consejo Superior de Investigaciones Científicas (CSIC), C/ Nicolás Cabrera, 13-15, Campus Cantoblanco, UAM, 28049 Madrid, Spain
Full list of author information is available at the end of the article

Abstract

Let g_t be a loop in the space of monic complex polynomials in one variable of fixed degree n. If the roots of g_t are distinct for all t, they form a braid B_1 on n strands. Likewise, if the critical points of g_t are distinct for all t, they form a braid B_2 on $n-1$ strands. In this paper we study the relationship between B_1 and B_2. Composing the polynomials g_t with the argument map defines a pseudo-fibration map on the complement of the closure of B_1 in $\mathbb{C}\times S^1$, whose critical points lie on B_2. We prove that for B_1 a T-homogeneous braid and B_2 the trivial braid this map can be taken to be a fibration map. In the case of homogeneous braids we present a visualization of this fact. Our work implies that for every pair of links L_1 and L_2 there is a mixed polynomial $f:\mathbb{C}^2\to\mathbb{C}$ in complex variables u, v and the complex conjugate $\overline{v}$ such that both f and the derivative f_u have a weakly isolated singularity at the origin with L_1 as the link of the singularity of f and L_2 as a sublink of the link of the singularity of f_u.

Keywords: Homogeneous braid, Isolated singularity, P-fibered braid, Real algebraic link, Saddle point braid, Braided open book

Mathematics Subject Classification: 57K10, 30C10, 32S55, 14P25, 14J17

1 Introduction

The braid group on n strands can be defined as the fundamental group of the space of monic, complex polynomials in one variable, of degree n and with distinct roots. In this way braids offer a close connection between algebraic geometry and topology. In this paper we illustrate how this connection is beneficial in both directions. We use topological arguments to prove that there exist polynomial maps with singularities and prescribed topological properties and we use insights on polynomial maps to obtain visualizations of certain topological phenomena. Our hope is that we may encourage further research interactions between the two areas.

One well-known intersection of the two areas is the study of links of isolated singularities of polynomial maps. Let $f:=(f_1,f_2):\mathbb{R}^4\to\mathbb{R}^2$ be a real polynomial map in variables x_1,x_2,x_3 and x_4 that satisfies $f(0,0,0,0)=(0,0)$ and $\frac{\partial f_i}{\partial x_j}(0,0,0,0)=0$ for all $i=1,2, j=1,2,3,4$. A critical point of f is a point x in $\mathbb{R}^4$ where the Jacobian matrix $\nabla f(x)=\left(\frac{\partial f_i}{\partial x_j}(x)\right)_{i,j}$ does not have full rank. We denote the set of critical points of f by Σ_f and the set of zeros of f,

i.e., all $x \in \mathbb{R}^4$ with $f(x) = (0, 0)$, by V_f. In particular, we have $(0, 0, 0, 0) \in \Sigma_f \cap V_f$. We say that f has a *weakly isolated singularity* at the origin if there is a neighborhood U of the origin in $\mathbb{R}^4$ such that $U \cap \Sigma_f \cap V_f = \{(0, 0, 0, 0)\}$. In other words, the rank of $\nabla f(0, 0, 0, 0)$ should be 0, but for all other $x \in U \cap V_f \backslash \{(0, 0, 0, 0)\}$ the rank of $\nabla f(x)$ should be 2.

Let S^3_ρ denote the Euclidean 3-sphere of radius ρ, centered at the origin. If f has a weakly isolated singularity at the origin, then the intersection of V_f and S^3_ρ results in a closed 1-dimensional submanifold, a link, if ρ is chosen sufficiently small. Furthermore, the link type of $L_f := V_f \cap S^3_\rho$, that is, its ambient isotopy class in S^3, is independent of the radius ρ, as long as ρ is sufficiently small. This link is thus a topological property of the singularity. We call L_f the link of the singularity.

The name *weakly* isolated singularity is justified in the sense that it does not impose any restrictions on the link types that arise in this way. Akbulut and King proved that every link is the link of a weakly isolated singularity of some real polynomial map [1]. However, there is also a stronger notion of isolation. We say that the origin is an *isolated singularity* of f if there is a neighborhood U of the origin in $\mathbb{R}^4$ such that $U \cap \Sigma_f = \{(0, 0, 0, 0)\}$. So the rank of $\nabla f(0, 0, 0, 0)$ should be 0, but for all other $x \in U \backslash \{(0, 0, 0, 0)\}$ the rank of $\nabla f(x)$ should be 2. Naturally, isolated singularities are weakly isolated. A link type is called *real algebraic* if it arises as the link of an isolated singularity of some real polynomial map.

The definitions above generalize to other dimensions as well as to complex polynomial maps. While links of isolated singularities of complex plane curves $f : \mathbb{C}^2 \to \mathbb{C}$ are completely classified, it is not known which links are real algebraic.

A link L in S^3 is called *fibered* if it is the binding of an open book decomposition of S^3. In other words, there is a fibration map $\varphi : S^3 \backslash L \to S^1$ with a specified behavior on a tubular neighborhood of L. The term *fibration* means that φ has no critical points, i.e., no points $x \in S^3 \backslash L$, where the directional derivatives of φ in any three linearly independent directions are all 0. The required behavior of φ on the tubular neighborhood $N(L)$ of L is as follows. Every connected component of $N(L)$ is an open solid torus. Removing L leaves $S^1 \times (D \backslash \{0\})$, where D denotes the open (unit) disk in $\mathbb{C}$. On $S^1 \times (D \backslash \{0\})$ we require that $\varphi(t, z) = \arg(z)$, where arg denotes the argument map that sends a nonzero complex number z to $\frac{z}{|z|}$.

The set of fibered links is a promising candidate for the still unknown set of real algebraic links. Milnor proved that all real algebraic links are fibered [28], while Benedetti and Shiota conjecture that the two sets of links are identical [3].

In the last couple of years several constructions of polynomials with isolated singularities have been proposed [7,10,13]. These have not resulted in a proof of Benedetti's and Shiota's conjecture, but we now have several infinite families of fibered links that are known to be real algebraic. All of these constructions are based on braids and produce so-called *semiholomorphic polynomials*. This means that when the constructed real polynomial map $f : \mathbb{R}^4 \to \mathbb{R}^2$ is written as a *mixed polynomial* $f : \mathbb{C}^2 \to \mathbb{C}$ in complex variables u, v and their complex conjugates $\bar{u}$ and $\bar{v}$ (which is clearly possible for any real polynomial map), then f is holomorphic with respect to u, i.e., $\frac{\partial f}{\partial \bar{u}} = 0$. From now on we write f_u for $\frac{\partial f}{\partial u}$.

With a similar construction we obtained the semiholomorphic version of Akbulut's and King's result: Every link type arises as the link of a weakly isolated singularity of a semiholomorphic polynomial [12]. One of the main results of this paper is an improvement on this construction. We may perform the construction from [12] to obtain the desired f

and obtain any given link L_2 as a sublink of the link of a singularity of f_u, i.e. L_2 is a subset of the connected components of L_{f_u}. We thus have a certain control not only over the topology of V_f but also over the topology of V_{f_u} at the same time.

Theorem 1.1 *Let L_1 and L_2 be links in S^3. Then there exists a semiholomorphic polynomial $f : \mathbb{C}^2 \to \mathbb{C}$ such that both f and f_u have a weakly isolated singularity at the origin with L_1 as the link of the singularity of f and L_2 a sublink of the link of the singularity of f_u.*

A *braid* on n strands is a set of disjoint parametric curves

$$\bigcup_{t\in[0,2\pi]} \bigcup_{j=1}^{n} (z_j(t), t) \subset \mathbb{C} \times [0, 2\pi], \tag{1}$$

where $z_j(t) : [0, 2\pi] \to \mathbb{C}$ are smooth functions with $z_i(t) \neq z_j(t)$ for all $t \in [0, 2\pi]$ and all $i \neq j$. Furthermore, for every index i there should be an index j with $z_i(0) = z_j(2\pi)$. Since the curves are parametrized by the height coordinate t, no strand can loop back and cross itself. The parametrization induces an orientation on the braid. Writing $\gamma_j(t)$ for the curve $(z_j(t), t)$, the tangent vector $\gamma'(t)$ has a positive coefficient of ∂_t, namely $+1$. We say that the curves are *positively transverse* to the horizontal planes $\mathbb{C} \times \{t\}$ for all $t \in [0, 2\pi]$. Occasionally, we might encounter a set of parametric curves B in $\mathbb{C} \times [0, 2\pi]$ that are transverse to all of these planes, but that are not parametrized by t itself. In this case there is a choice of orientation for B so that is a braid, but it might not match the orientation induced by the parametrization. We could thus consider B as an unoriented braid.

A braid isotopy is an isotopy of a braid in $\mathbb{C} \times [0, 2\pi]$ that fixes the start- and endpoints at $t = 0$ and $t = 2\pi$, and maintains the braid property throughout the isotopy. Often a braid isotopy class is also called a braid. When we want to emphasize that we are referring to a representative of an isotopy class instead of the isotopy class itself, we usually call the representative a geometric braid.

Fixing the start- and endpoints $z_i(0)$ we obtain a group structure on the set of isotopy classes of braids on n strands, where the group operation is given by concatenation and rescaling of the interval. This way we may interpret the braid group on n strands $\mathbb{B}_n$ as the fundamental group of the configuration space C_n of n distinct, unmarked points in the complex plane, where the chosen set of start- and endpoints $z_i(0)$ corresponds to the basepoint of the loop. C_n is thus given by the quotient $(\mathbb{C}^n \backslash \Delta)/S_n$, where Δ is the set of n-tuples where at least two entries are identical and S_n is the symmetric group on n elements acting on n-tuples by permutation. The space $(\mathbb{C}^n \backslash \Delta)$ is an open subset of $\mathbb{C}^n$ with the smooth structure of its ambient space $\mathbb{R}^{2n} \cong \mathbb{C}^n$. By the Quotient Manifold Theorem (e.g., [23]) the quotient space C_n inherits a unique smooth structure so that the quotient map is a smooth submersion.

By the fundamental theorem of algebra the space X_n of monic polynomials in one complex variable of degree n and with distinct roots is in bijection with C_n. This correspondence identifies an unordered n-tuple $\{z_1, z_2, \ldots, z_n\} \in C_n$ with the polynomial $g : \mathbb{C} \to \mathbb{C}, g(u) := \prod_{j=1}^{n} (u - z_j)$.

The smooth structure on C_n thus gives a smooth structure on X_n, so that the bijection established by the fundamental theorem of algebra is a diffeomorphism.

Every geometric braid, parametrized as in Eq. (1), is a loop in C_n and thus corresponds to a loop in X_n, given by $g_t : \mathbb{C} \to \mathbb{C}$,

$$g_t(u) = \prod_{j=1}^{n}(u - z_j(t)). \tag{2}$$

Conversely, the roots of any smooth loop in this space X_n of polynomials form a geometric braid on n strands.

The natural smooth structure on X_n explained above matches common intuition as follows. Since the coefficients of a polynomial are smooth functions of its roots (with a smooth local inverse if the roots are distinct), a loop

$$g_t(u) = \prod_{j=1}^{n}(u - z_j(t)) = u^n + \sum_{j=0}^{n-1} a_j(t)u^j \tag{3}$$

in X_n is smooth if and only if its coefficients $a_j(t), j = 1, 2, \ldots, n-1$, are smooth functions of t, which occurs if and only if the strands of the corresponding braid are parametrized by smooth functions $z_j(t), j = 1, 2, \ldots, n$ [18].

This paper focuses on a subset of this space of polynomials X_n. We define $\widehat{X}_n$ to be the space of monic polynomials of degree n with distinct roots, distinct critical values and constant term not equal to any of its critical values. If the critical values are distinct, so are the critical points. Since the critical points of a complex polynomial g in one variable u are exactly the roots of $\frac{\partial g}{\partial u}$, which is a polynomial of degree $n-1$, it follows that we can associate to every loop g_t in $\widehat{X}_n$ three braids: one braid on n strands that is formed by the roots of g_t, one braid that is formed by the critical values and one braid on $n-1$ strands that is formed by the critical points of g_t. The relation between the braid that is formed by the roots of a loop in $\widehat{X}_n$ with constant term equal to 0, and the braid that is formed by its critical values was studied in detail in [9].

By holomorphicity each critical point of a polynomial p in $\widehat{X}_n$ must also be a critical point of $\arg(p)$. Furthermore, it is a saddle point of $\arg(p)$, that is, it is neither a local maximum nor a local minimum. For this reason we also call the braid that is formed by the critical points of g_t the *saddle point braid* of g_t. One major topic of this article is the relation between the braid formed by the roots and the saddle point braid of a given loop of polynomials g_t in $\widehat{X}_n$. We prove that any pair of braids can be realized as the roots and saddle point braid of an appropriate loop of polynomials.

Theorem 1.2 *Let B and B' be braids on n and $n-1$ strands, respectively. Then there is a loop $g_t : \mathbb{C} \to \mathbb{C}$ in $\widehat{X}_n$ such that*

- *the roots $\{(u,t) \in \mathbb{C} \times [0, 2\pi] | g_t(u) = 0\}$ form the braid B,*
- *the saddle point braid, given by $\{(u,t) \in \mathbb{C} \times [0, 2\pi] | \frac{\partial g_t}{\partial u}(u) = 0\}$, is B'.*

Theorem 1.2 is related to work in [38], where it was shown that not every braid can be realized as the union of roots and saddle point braid of some loop of polynomials, even when certain immediate convexity constraints are taken into account. So by Theorem 1.2 we can control the topology of the braid of roots B and the saddle point braid B' at the same time, but we do not have control over the braid type of their union, which is a braid on $2n-1$ strands.

At almost every height $t \in [0, 2\pi]$ we may order the strands of a braid at that height by the real parts of their complex coordinate. That is, if $\bigcup_{j=1}^{n}(z_j(t), t)$, then the first strand at height $t = t_*$ is the strand with smallest $\mathrm{Re}(z_j(t_*))$. The second strand has the next smallest value of $\mathrm{Re}(z_j(t_*))$ and so on. The braid group on n strands is generated by the Artin generators σ_i, $i = 1, 2, \ldots, n-1$, which correspond to positive half-twists between the ith strand and the $(i+1)$st strand.

Definition 1.3 A braid $B = \prod_{j=1}^{\ell} \sigma_{i_j}^{\varepsilon_j}$ on n strands is called *homogeneous* if

i) for every $k \in \{1, 2, \ldots, n-1\}$ there is a $j \in \{1, 2, \ldots, \ell\}$ with $i_j = k$,
ii) for every $j, j' \in \{1, 2, \ldots, \ell - 1\}$, $i_j = i_{j'}$ implies $\varepsilon_j = \varepsilon_{j'}$.

In other words, a braid is homogeneous if for all $i \in \{1, 2, \ldots, n-1\}$ its word contains the generator σ_i if and only if it does not contain its inverse σ_i^{-1}. In the literature (in particular in [36]) braids are sometimes called homogeneous if they satisfy the second condition above and *strictly homogeneous* if they satisfy both conditions above.

Since the start- and endpoints of any geometric braid B match, we may identify the $t = 0$-plane and the $t = 2\pi$-plane to obtain a link in $\mathbb{C} \times S^1$. Embedding this open solid torus as an untwisted neighborhood of a planar circle in S^3 results in a well-defined link in S^3, the closure of the braid B, whose ambient isotopy class in S^3 does not depend on the representative of the braid isotopy class of B.

Stallings showed that closures of homogeneous braids are fibered links [40]. In fact Definition 1.3 has a generalization in the form of T-homogeneous braids, which were introduced and shown to close to fibered links by Rudolph [36]. In Sect. 2 we will review the definition and some properties of T-homogeneous braids.

We say that a geometric braid B parametrized by $\bigcup_{j=1}^{n}(z_j(t), t)$ is *P-fibered* (short for "fibered via polynomials") if the corresponding loop of polynomials $g_t(u) = \prod_{j=1}^{n}(u - z_j(t))$ defines an explicit fibration map via $\arg(g) : (\mathbb{C} \times S^1) \backslash B \to S^1$, where $g : \mathbb{C} \times S^1 \to \mathbb{C}$, $g(u, e^{it}) = g_t(u)$. We say that a braid isotopy class is P-fibered if it has a P-fibered representative. Sometimes this condition is weakened to require a P-fibered representative in its conjugacy class in $\mathbb{B}_n$. Closures of P-fibered braids are fibered links in S^3 [10], but it is not known if every fibered link is the closure of a P-fibered braid.

T-homogeneous braids are P-fibered [11,36] and closures of T-homogeneous braids have also recently been proved to be real algebraic [13]. We prove that the loop of polynomials that realizes a T-homogeneous braid as a P-fibered braid can be taken to have a trivial saddle point braid.

Theorem 1.4 *Let B be a T-homogeneous braid on n strands. Then there is a loop $g_t : \mathbb{C} \to \mathbb{C}$ in $\widehat{X}_n$ such that*

- *the roots $\{(u, t) \in \mathbb{C} \times [0, 2\pi] | g_t(u) = 0\}$ trace out the braid B,*
- *$(u, t) \mapsto g_t(u) \mapsto \arg g_t(u)$ is a fibration of $(\mathbb{C} \times S^1) \backslash B$ over S^1,*
- *the saddle point braid, given by $\{(u, t) \in \mathbb{C} \times [0, 2\pi] | \frac{\partial g_t}{\partial u}(u) = 0\}$, is the trivial braid on $n - 1$ strands.*

The condition that the map $(u, t) \mapsto \arg g_t(u)$ is a fibration means that it does not have any critical points. If the map $(u, t) \mapsto \arg g_t(u)$ for a given loop of polynomials g_t has a

finite number of non-degenerate critical points, i.e., it is a circle-valued Morse map, we call it a pseudo-fibration.

A construction similar to the one employed in [13] results in the following theorem.

Theorem 1.5 *Let L be the closure of a T-homogeneous braid B on n strands. Then there is a semiholomorphic polynomial $f : \mathbb{C}^2 \to \mathbb{C}$ such that f has an isolated singularity at the origin with link L and f_u has a weakly isolated singularity at the origin whose link is the unlink with $n-1$ components.*

The structure of the rest of the article is as follows. Section 2 reviews some properties of loops of polynomials in $\widehat{X}_n$, resulting in a proof of Theorem 1.4 and Theorem 1.2. We also give a new upper bound on the Morse–Novikov number of a link, the minimal number of critical points of a pseudo-fibration. In Sect. 3 we modify the constructions of (weakly) isolated singularities from [12] and [13] to prove Theorem 1.1 and Theorem 1.5. In appendix (Sect. Appendix 1) we then study the argument map $\arg(g_t)$ of a loop of polynomials g_t in $\widehat{X}_n$ and offer different visualizations of the fibration for homogeneous braids as well as of pseudo-fibrations for general braids.

2 Saddle point braids

The space $\widehat{X}_n$ of monic polynomials of fixed degree n and distinct roots, distinct critical values and constant term different from all critical values is defined in such a way that both the roots and the critical points of a loop in $\widehat{X}_n$ form a (closed) braid in $\mathbb{C} \times S^1$. A parametrization $z_j(t), j = 1, 2, \ldots, n$, of the roots can be easily obtained by decomposing the polynomials into their irreducible factors, i.e. $g_t(u) = \prod_{j=1}^{n}(u - z_j(t))$. Likewise, the critical points of a loop g_t, which form the saddle point braid, are given by $\bigcup_{j=1}^{n-1}(c_j(t), t)$ where $\frac{\partial g_t}{\partial u}(u) = n\prod_{j=1}^{n-1}(u - c_j(t))$. The relation between these polynomials is then obviously $g_t(u) = \int_0^u \frac{\partial g_t}{\partial u}(w)\mathrm{d}w$.

We may write $v_j(t) = g_t(c_j(t)), j = 1, 2, \ldots, n-1$, for the critical values of g_t. The relation between the braid that is parametrized by the v_j (or more precisely the union of the v_j and $\{0\} \times [0, 2\pi]$) and the braid that is formed by the roots of g_t was the object of study in [9]. One aspect that continues to be relevant in this paper is that deformations of the braid of critical values lift to deformations in $\widehat{X}_n$ and thus also to deformations of the braid of roots and the saddle point braid.

More precisely, we may write

$$V_n := \{(v_1, v_2, \ldots, v_{n-1}) \in (\mathbb{C}\backslash\{0\})^{n-1} : v_i \neq v_j \text{ if } i \neq j\}/S_{n-1}, \tag{4}$$

for the space of critical values of polynomials in $\widehat{X}_n$, where the symmetric group S_{n-1} acts on $n-1$-tuples of non-zero complex numbers by permutation. Note that the critical values are nonzero, since polynomials in $\widehat{X}_n$ have distinct roots. We then define

$$\widehat{V}_n := \{(v, a_0) \in V_n \times \mathbb{C} : a_0 \neq v_j \text{ for all } j\}. \tag{5}$$

Then by Corollary 2.20 in [11] the map θ_n that sends a polynomial in $\widehat{X}_n$ to its set of critical values $v \in V_n$ and its constant term a_0 is a covering map of degree n^{n-1}.

Suppose now that g_t is a loop in $\widehat{X}_n$ and let v_t denote the loop of the corresponding critical values. That is, if we denote the projection map $\widehat{V}_n \to V_n$ by π, we have $v_t = \pi(\theta_n(g_t))$.

Any homotopy of v_t in V_n is a braid isotopy that therefore extends to an ambient isotopy and gives a homotopy of $\theta_n(g_t)$ in $\widehat{V}_n$, which then lifts to a homotopy of g_t in $\widehat{X}_n$. By definition of $\widehat{X}_n$ the braid type of the braid formed by the roots and the braid type of the saddle point braid do not change during this homotopy.

The relation between the braid formed by the roots and the braid formed by the critical values is important in the context of fibrations.

Recall that the property that $\arg(g)$ is a fibration map means that it does not have any critical points. By [10] $(u_*, t_*) \in (\mathbb{C} \times S^1)\backslash B$ is a critical point of $\arg(g)$ if and only if $\frac{\partial g}{\partial u}(u_*, t_*) = \frac{\partial \arg(g)}{\partial t}(u_*, t_*) = 0$. This implies that all critical points must lie on the saddle point braid, i.e., there is some $j \in \{1, 2, \ldots, n-1\}$ such that $c_j(t_*) = u_*$, where $c_j(t)$, $j = 1, 2, \ldots, n-1$, parametrize the saddle point braid. The property of being P-fibered is therefore also equivalent to $\frac{\partial \arg(v_j(t))}{\partial t} \neq 0$ for all j and all t, which has the geometric interpretation that each critical value $v_j(t)$, interpreted as a curve $(v_j(t), t)$ in $\mathbb{C} \times [0, 2\pi]$, has a fixed orientation (clockwise or counter-clockwise) with which it twists around $0 \times [0, 2\pi] \subset \mathbb{C} \times [0, 2\pi]$.

We now define a particular family of P-fibered braids, the T-homogeneous braids, which feature in Theorems 1.4 and 1.5. They are a generalization of the homogeneous braids defined in Definition 1.3.

Let $\mathscr{T}$ be an embedded tree graph in the complex plane with n vertices. Furthermore, every edge e of $\mathscr{T}$ should be associated with a sign $\varepsilon_e \in \{+, -\}$. See Fig. 1a for an example. After a planar isotopy of $\mathscr{T}$ we may assume that the vertices of $\mathscr{T}$ are the n roots of a complex polynomial in $\widehat{X}_n$. We consider loops in $\widehat{X}_n$ whose basepoint is given by the n-tuple of the vertices of $\mathscr{T}$. For every edge e there is a loop $g_e^{\varepsilon_e}$ in $\widehat{X}_n$ that exchanges the endpoints of the edge, where the sign of the twist matches ε_e as in Fig. 1b. Note that every twist occurs in a neighborhood of the edge. A braid on n strands is called $\mathscr{T}$-homogeneous if it has a representative of the form $g_t = \prod_{j=1}^{\ell} g_{e_j}^{\varepsilon_{e_j}}$, where for every edge e there is an index $j \in \{1, 2, \ldots, \ell\}$ with $e_j = e$. Here $\prod$ refers to the concatenation of loops, not a product of polynomials. The order in which the twists occur or the number of times each twist occurs is not relevant for this definition. In general we say that a braid B is T-homogeneous if there is some embedded tree $\mathscr{T}$ with choice of signs ε_e, such that B is $\mathscr{T}$-homogeneous with respect to $\mathscr{T}$ and the chosen signs. Figure 1c shows an example of a $\mathscr{T}$-homogeneous braid for the embedded tree in Fig. 1a. Here and in all figures of braids in this article where a braid is drawn vertically, t is increasing from 0 to 2π as we go from the bottom to the top of the picture.

Every homogeneous braid B is $\mathscr{T}$-homogeneous, if $\mathscr{T}$ is the line graph. Numbering the edges from left to right means that the sign ε_j of the edge $j \in \{1, 2, \ldots, n-1\}$ is the unique sign with which σ_j appears in the homogeneous braid word B.

We now explain how embedded trees arise naturally in the study of complex polynomials. Let $p : \mathbb{C} \to \mathbb{C}$ be a complex polynomial in $\widehat{X}_n$ with critical values $v_k, k = 1, 2, \ldots, n-1$, such that $\arg(v_i) \neq \arg(v_j)$ for all $i \neq j$. Then the argument map $\arg(p)$ induces a singular foliation on $\mathbb{C}$ whose leaves are connected components of level sets of $\arg(p)$. The singular foliation has two types of singularities; elliptic singularities, which are the roots of p, and hyperbolic singularities, which are the critical points of p. Every singular leaf of this foliation has the shape of a cross, consisting of one line connecting two roots of p and one

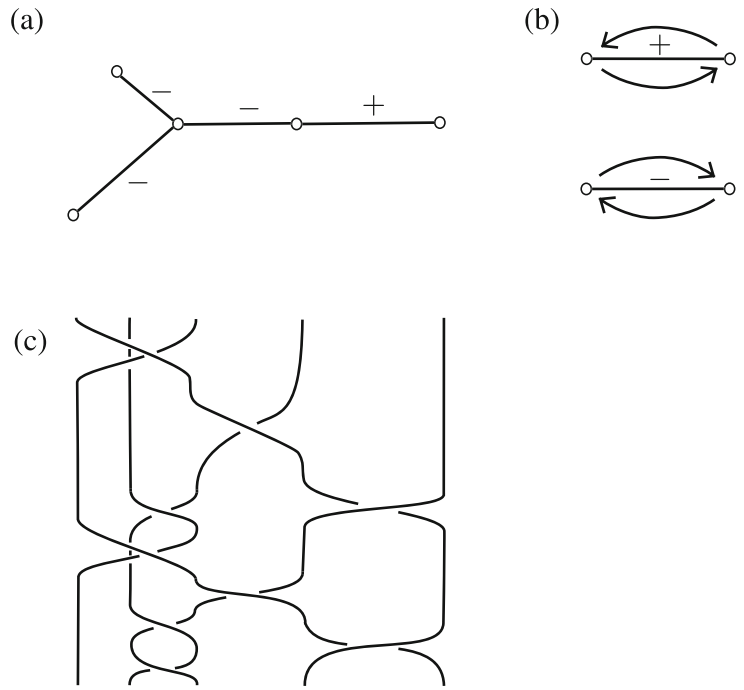

Fig. 1 **a** An embedded tree $\mathscr{T}$ in the complex plane. The signs ε_e are drawn on each edge e. **b** The loop g_e exchanges the roots on the endpoints of e as in the upper picture if $\varepsilon_e = +1$ and as in the lower picture if $\varepsilon_e = -1$. **c** A $\mathscr{T}$-homogeneous braid with $\mathscr{T}$ as in Subfigure (**a**) with t increasing from 0 to 2π from the bottom to the top

going to the circle boundary $\partial D = S^1$ of $\mathbb{C} \cong D$. The two lines meet in a critical point of p.

The nth roots of unity divide $\partial D = S^1$ into n arcs. We denote the arcs by A_j, $j = 1, 2, \ldots, n$, increasing the label as we go around the circle clockwise. The choice of arc that is labeled A_1 is arbitrary, but it should be the same for all polynomials p. Let c_k, $k = 1, 2, \ldots, n-1$ be the critical points of p with $v_k = p(c_k)$. Since the roots of p are distinct, $v_k \neq 0$ for all k. We may assume that $0 < \arg(v_1) < \arg(v_2) < \ldots < \arg(v_{n-1}) < 2\pi$.

We may then associate to each critical point c_k (or to each critical value $v_k = p(c_k)$) a transposition $\tau_k \in S_n$, where S_n denotes the permutation group on n elements. As mentioned above, c_k lies on a unique singular leaf of the singular foliation of D induced by $\arg(p)$. This singular leaf has two endpoints on $\partial D = S^1$ that lie on two different arcs A_i and A_j, $i \neq j$. Then $\tau_k = (i\, j)$. It turns out that every such list of ordered transpositions τ_k satisfies $\prod_{k=1}^{n-1} \tau_k = (1\ 2\ \ldots\ n-1\ n)$. The ordered list $\{\tau_k\}_{k\in\{1,2,\ldots,n-1\}}$ is called the *cactus* of the polynomial p, see [11,13,20] for more details. Note that labeling the arcs A_j clockwise is the convention from [13], which is the opposite of that of [11].

The definition of τ_k is illustrated in Fig. 2a. In Fig. 2b we show the singular leaves of the singular foliation induced by $\arg(p)$, where p is a polynomial of degree 4. The regular leaves can easily be filled in, since they always connect a root to the boundary circle. The cactus of the displayed polynomial is $\tau_1 = (1\ 4)$, $\tau_2 = (2\ 4)$, $\tau_3 = (3\ 4)$.

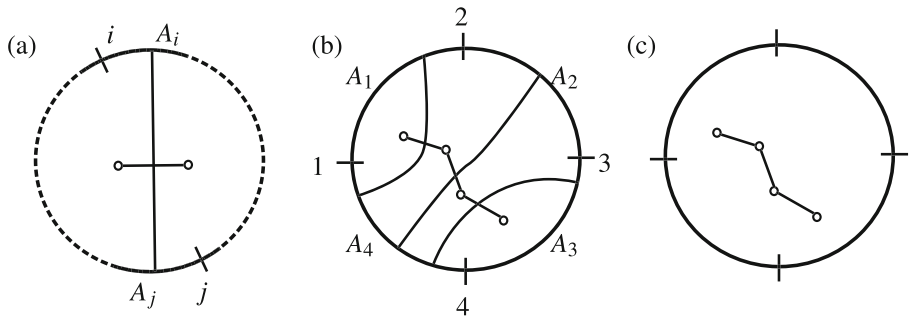

Fig. 2 Defining the cactus of a polynomial p from the singular foliation induced by $\arg(p)$. **a** A singular leaf with a critical point c_k with $\tau_k = (i\,j)$. **b** The singular leaves of the singular foliation induced by $\arg(p)$. **c** The embedded tree associated with a polynomial p

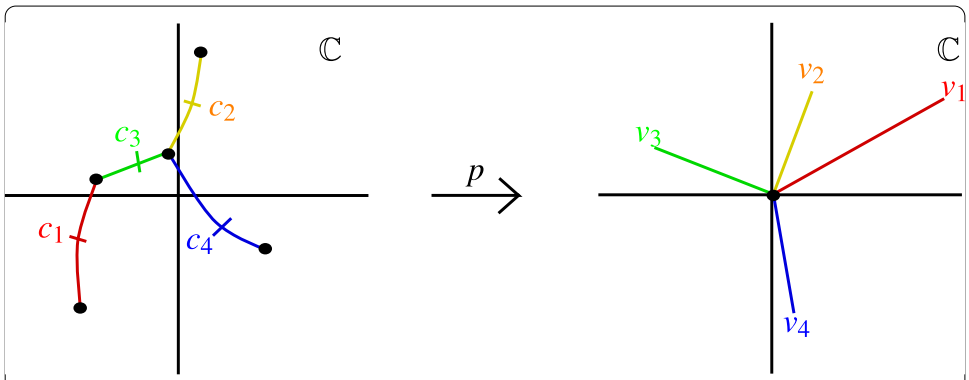

Fig. 3 Planar tree graph associated with a polynomial p is mapped to a star graph by p

We may also associate with p in $\widehat{X}_n$ a planar graph embedded in $\mathbb{C}$, whose vertices are the roots of p and whose edges are the parts of the singular leaves that connect two roots, see Fig. 2c. This combinatorial structure is essentially equivalent to the cactus of the polynomial p. The resulting graph is always a tree and up to planar isotopy every embedded tree arises in this way.

Let $\mathscr{T}$ be the embedded tree associated with a polynomial p in $\widehat{X}_n$. Suppose that the critical values v_j, $j = 1, 2, \ldots, n-1$, all have distinct arguments. Then the image of $\mathscr{T}$ under p is a star graph with $n-1$ edges. Since the vertices of $\mathscr{T}$ are by definition the roots of p, they all get mapped to the origin in $\mathbb{C}$. Every edge of $\mathscr{T}$ contains a unique critical point c_j and by definition $\arg(p)$ is constant along each edge of $\mathscr{T}$, so that the image of each edge of $\mathscr{T}$ is a straight line from the origin in $\mathbb{C}$ to the corresponding critical value $v_j = p(c_j)$, see Fig. 3.

There is a connection between embedded trees and subsets of the BKL-generators $a_{i,j}$, $i, j \in \{1, 2, \ldots, n\}$, $i \neq j$, which were introduced by Birman, Ko and Lee in [5], and which also generate $\mathbb{B}_n$. The generator $a_{i,j}$ represents a positive half-twist between the ith strand and the jth strand such that in the projection the twist lies in front of all strands whose indices are between i and j. See Fig. 4 for an example. In particular, the Artin generator σ_i is given by $a_{i,i+1}$. BKL-generators (or band generators as they are also called) are often used to describe braided surfaces in $\mathbb{C} \times [0, 2\pi]$, where each strand corresponds to a disk and each generator $a_{i,j}$ to a half-twisted band between the ith and the jth disk. In this way

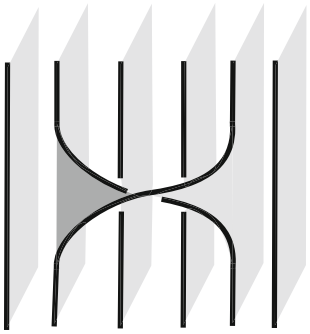

Fig. 4 Band generator $a_{2,5}$

a word in the BKL-generators describes a surface whose boundary is the corresponding braid represented by the same BKL-word.

For every embedded tree $\mathscr{T}$ the twists g_{e_j} around edges $e_j, j = 1, 2, \ldots, n-1$, generate the braid group on n strands, where n is the number of vertices of $\mathscr{T}$, see [36]. After a planar isotopy of $\mathscr{T}$ (which does not change the set of corresponding $\mathscr{T}$-homogeneous braids up to conjugacy) these generators can be realized as a subset of the band generators or BKL-generators [5,36]. We call the set $S_{\mathscr{T}}$ of BKL-generators associated with a given embedded tree $\mathscr{T}$ the $\mathscr{T}$-generators. This means that we can define the set of $\mathscr{T}$-homogeneous braids analogously to Definition 1.3. Naturally this definition is equivalent to the one explained above in terms of embedded trees and twists around edges.

Definition 2.1 Let $S_{\mathscr{T}} = \{s_1, s_2, \ldots, s_{n-1}\}$ be the set of $\mathscr{T}$-generators of $\mathbb{B}_n$ for some embedded tree $\mathscr{T}$ in $\mathbb{C}$. Let $B = \prod_{j=1}^{\ell} s_{i_j}^{\varepsilon_j}$ be a braid word in the $\mathscr{T}$-generators. Then B is a $\mathscr{T}$-homogeneous braid word if

i) for every $k \in \{1, 2, \ldots, n-1\}$ there is a $j \in \{1, 2, \ldots, \ell\}$ with $i_j = k$,
ii) for every $j, j' \in \{1, 2, \ldots, \ell - 1\}$, $i_j = i_{j'}$ implies $\varepsilon_j = \varepsilon_{j'}$.

We say that a braid B is *T-homogeneous* if there exists an embedded tree $\mathscr{T}$ with $\mathscr{T}$-generators $S_{\mathscr{T}}$ such that B can be represented by a $\mathscr{T}$-homogeneous braid word. Thus the set of T-homogeneous braids is the union of all $\mathscr{T}$-homogeneous braids, where the union is taken over all embedded trees $\mathscr{T}$ in $\mathbb{C}$.

Clearly, Definition 2.1 reduces to Definition 1.3 if $\mathscr{T}$ is taken to be the line graph and $S_{\mathscr{T}}$ is the set of Artin generators.

In [15] we introduced the inhomogeneity $\beta(B)$ of a braid B, a natural number that measures how far away a given braid word B in Artin generators is from being homogeneous. In particular, $\beta(B) = 0$ if and only if B is a homogeneous braid.

We may now define for every embedded tree $\mathscr{T}$ the $\mathscr{T}$-inhomogeneity $\beta_{\mathscr{T}}(B)$ of a braid B as follows. Denote the $\mathscr{T}$-generators by $s_1, s_2, \ldots, s_{n-1}$. Then express B as a word in these generators $B = \prod_{j=1}^{\ell} s_{i_j}^{\varepsilon_j}$. Then we count for each $i \in \{1, 2, \ldots, n-1\}$ the number of sign changes of the generator s_i as we traverse the braid word cyclically. We add all these numbers and add 2 for every generator that does not appear in the braid word at all,

neither with a positive nor with a negative sign. This is expressed as

$$\begin{aligned}\beta_{\mathscr{T}}(B) = \sum_{i=1}^{n-1} |\{j \in \{1,2,\dots,\ell-1\} : \exists k \in \{1,2,\dots,\ell-1\} \text{ s.t. } i_j = i_{j+k \bmod \ell} = i,\\ i_{j+m \bmod \ell} \neq i \text{ for all } m < k \text{ and } \varepsilon_j \varepsilon_{j+k \bmod \ell} = -1\}|\\ + 2|\{j \in \{1,2,\dots,n-1\} : \text{ There is no } k \text{ s.t. } i_k = j\}|. \end{aligned} \tag{6}$$

If $\mathscr{T}$ is the line graph, the $\mathscr{T}$-generators are the usual Artin generators and $\beta_{\mathscr{T}}(B) = \beta(B)$. Note that by definition $\beta_{\mathscr{T}}(B) = 0$ if and only B is a $\mathscr{T}$-homogeneous braid word. We should interpret $\beta_{\mathscr{T}}(B)$ as a property of a braid word. Of course, we may take any braid, inflate its word artificially by inserting arbitrarily many copies of $s_j s_j^{-1}$ and thereby make $\beta_{\mathscr{T}}(B)$ arbitrarily large. If we wanted to insist on a topological invariant, we would thus have to take the minimum over all braid words representing the same braid B. For practical purposes, it is of course much simpler to consider $\beta_{\mathscr{T}}(B)$ as a function from the set of words in $\mathscr{T}$-generators (and their inverses) to the natural numbers.

In order to prove Theorem 1.4 we need to find a loop of polynomials g_t in $\widehat{X}_n$ whose roots form a given T-homogeneous braid B, realized as a P-fibered geometric braid, and such that its saddle point braid is the trivial braid on $n-1$ strands. Loops of polynomials that realize B as a P-fibered geometric braid have been constructed in [11,36] and to some extent (for homogeneous braids) already in [6,8,35]. However, these articles do not mention the saddle point braid in this context. We quickly review the main steps in this construction and explain why the corresponding saddle point braid is the trivial braid.

Proposition 2.2 *Let $\mathscr{T}$ be an embedded tree in $\mathbb{C}$ with n vertices and let B be a word in the $\mathscr{T}$-generators. Then there is a loop g_t in $\widehat{X}_n$ such that the roots of g_t form the braid B, its saddle point braid is the trivial braid on $n-1$ strands and* $\arg(g) : (\mathbb{C} \times S^1) \backslash B \to S^1$, $\arg(g)(u, e^{it}) := \arg(g_t(u))$, *has exactly $\beta_{\mathscr{T}}(B)$ critical points.*

Proof After a planar isotopy of $\mathscr{T}$ we may assume that $\mathscr{T}$ is exactly the embedded tree associated with the polynomial $p(u) := \prod_{j=1}^{n}(u - z_j)$ (see, for example, Theorem 5.3 in [11]), where $z_1, z_2, \dots, z_n$ are the vertices of $\mathscr{T}$. We now study the loop of polynomials in $\widehat{X}_n$ whose roots form B and that has p as a basepoint.

Each $\mathscr{T}$-generator s_j corresponds to a twist g_{e_j} along an edge e_j of $\mathscr{T}$. Thus B is a concatenation of twists g_{e_j} along edges e_j of $\mathscr{T}$, say $\prod_{k=1}^{\ell} g_{e_{j_k}}^{\varepsilon_k}$, where the product refers to concatenation of loops in $\widehat{X}_n$. Each twist g_{e_j} corresponds to a very particular motion of the critical values and the constant term in $\widehat{V}_n$.

Let $c_1, c_2, \dots, c_{n-1}$ be the critical points of p, let $v_j = p(c_j)$, $j = 1, 2, \dots, n-1$, be the critical values of p and let a_0 be its constant term. After a small deformation of the embedded graph we may assume that $\arg(v_i) \neq \arg(v_j)$ if $i \neq j$. After a translation of $\mathscr{T}$ in $\mathbb{C}$, which does not affect the critical values or the graph structure, we may further assume that one of the z_j is equal to 0 and so $a_0 = 0 \neq v_j$ for all j, so in particular, $p \in \widehat{X}_n$. Since $\mathscr{T}$ is the embedded tree associated with p, every edge of $\mathscr{T}$ contains exactly one critical point c_j of p. We may thus choose the indexing of the edges of $\mathscr{T}$ such that e_j contains c_j. There is now a one-to-one correspondence between edges of $\mathscr{T}$ and critical values of p, where an edge e_j corresponds to the critical value $v_j = p(c_j)$, see also Fig. 3. The twist $g_{e_j}(u)$ can be explicitly realized as a loop in $\widehat{X}_n$ via $p(u) - \gamma_j(t)$, where $\gamma_j(t)$ is a loop in $\mathbb{C}$ with basepoint

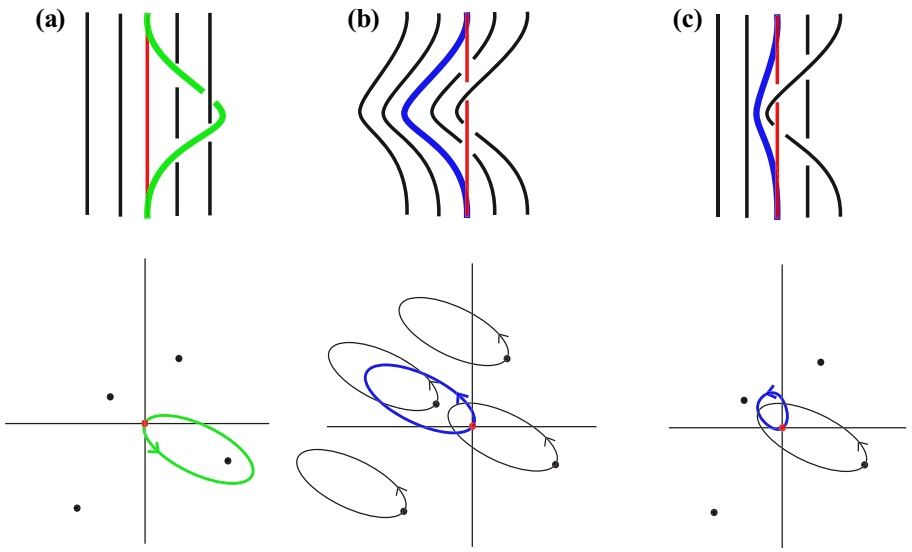

Fig. 5 **a** Critical values $v_j, j = 1, 2, \ldots, n-1$ (in black), the origin $0 \in \mathbb{C}$ (in red) and $\gamma_j(t)$ (in thick green), both as curves in $\mathbb{C} \times S^1$ and as motions in $\mathbb{C}$. **b** Curves $v_j - \gamma_j(t), j = 1, 2, \ldots, n-1$ (in black), the origin $0 \in \mathbb{C}$ (in red) and the constant term $-\gamma_j(t)$ (in thick blue), both as curves in $\mathbb{C} \times S^1$ and as motions in $\mathbb{C}$. **c** A deformation of the curves from Subfigure (**b**) so that all but one critical value become stationary

at the origin and the property that it encircles the critical value v_j counterclockwise in an ellipse that does not contain any other critical values v_i with $i \neq j$ as shown in Fig. 5a. We denote the inverse loop of $\gamma_j(t)$ that encircles v_j in a clockwise direction by $\gamma_j(t)^{-1}$. □

Thus we have realized B as the roots of a loop in $\widehat{X}_n$ that is given by $\prod_{k=1}^{\ell}(p - \gamma_{j_k}(t)^{\varepsilon_k})$, where again the product refers to concatenation of loops in $\widehat{X}_n$. Since the constant term is the only term that depends on t, the saddle point braid of the corresponding loop of polynomials is the trivial braid on $n-1$ strands.

The motion of the critical values of a loop g_{e_j} is shown in Fig. 5b. As in Fig. 5c we may deform the loop of critical values and constant term $-\gamma_j(t)$ such that $v_i(t)$ does not depend on t if $i \neq j$ and v_j encircles $\{0\} \times [0, 2\pi]$ counterclockwise in an ellipse. Thus the loop of critical values and constant term $\theta_n(\prod_{k=1}^{\ell}(p - \gamma_{j_k}(t)^{\varepsilon_k}))$ can be deformed in $\widehat{V}_n$ so that in each interval $t \in \left[\frac{2\pi(k-1)}{\ell}, \frac{2\pi k}{\ell}\right]$ the critical values $v_i(t)$ with $i \neq j_k$ do not depend on t, while v_{j_k} moves on an ellipse around the origin, going counterclockwise if $\varepsilon_k = 1$ and clockwise if $\varepsilon_k = -1$.

We may now deform the loop of critical values slightly to make $\partial_t \arg(v_i(t))$ nonzero for all $t \in \left[\frac{2\pi(k-1)}{\ell}, \frac{2\pi k}{\ell}\right]$ and all $i \neq j_k$. All of these deformations are homotopies in $\widehat{V}_n$ and lift to a homotopy of $\prod_{k=1}^{\ell}(p - \gamma_{j_k}(t)^{\varepsilon_k})$ in $\widehat{X}_n$. The resulting loop g_t in $\widehat{X}_n$ therefore still has the same braid of roots and the saddle point braid as $\prod_{k=1}^{\ell}(p - \gamma_{j_k}(t)^{\varepsilon_k})$, that is, B and the trivial braid on $n-1$ strands, respectively.

The corresponding braid of critical values consists of strands that are motions of points on ellipses. We know that critical points of $\arg(g)$ are exactly points where a critical value $v_i(t)$ changes its direction with which it moves on its ellipse, clockwise or counterclockwise. Since the direction of motion on the ellipse is given by the signs ε_k with $j_k = i$, this number

is exactly

$$|\{k \in \{1,2,\dots,\ell-1\} : \exists h \in \{1,2,\dots,\ell-1\} \text{ s.t. } j_k = j_{k+h \bmod \ell} = i, \\ j_{k+m \bmod \ell} \neq i \text{ for all } m < h \text{ and } \varepsilon_k \varepsilon_{k+h \bmod \ell} = -1\}|. \tag{7}$$

If there is no k with $j_k = i$, i.e., the $\mathscr{T}$-generator corresponding to g_{e_i} does not appear in the braid word with any sign, then $v_i(t)$ can be taken to be constant. In order to obtain a Morse function, we deform this stationary strand such that $\arg(v_i(t))$ has exactly two critical points. Thus the number of critical points of $\arg(g)$ is exactly $\beta_{\mathscr{T}}(B)$. □

Proof of Theorem 1.4 Let B be a $\mathscr{T}$-homogeneous braid for some embedded tree $\mathscr{T}$ with chosen signs. By definition $\beta_{\mathscr{T}}(B) = 0$ and so the theorem follows from Proposition 2.2. □

Fibered links in S^3 are exactly the bindings of open book decompositions of S^3. We say that an open book in S^3 is a braided open book if its binding is the closure of a P-fibered braid [11]. The braid axis can then be thought of as a braid axis for the entire open book, not only for the binding, that is, all fiber surfaces (the pages of the open book) are positioned in a very natural way relative to this braid axis. They are all braided surfaces in the sense of Rudolph [36].

An equivalent definition of braided open books in S^3 involves simple branched covers $S^3 \to S^3$. Montesinos and Morton conjecture that for every fibered link L in S^3 there is a simple branched cover $\Pi : S^3 \to S^3$ of degree n, branched over a link L_{branch} such that $L = \Pi^{-1}(\alpha)$ is the preimage of some braid axis α of L_{branch} and L_{branch} is the unlink on $n-1$ components [29].

We showed in [11] that we can construct a simple branched cover $\Pi : S^3 \to S^3$ from any loop of polynomials g_t, whose roots form a P-fibered geometric braid. The resulting branch link L_{branch} is exactly the closure of the braid that is formed by the critical values of g_t. The proof of Proposition 2.2 shows that for closures of T-homogeneous braids the conjecture by Montesinos and Morton is true, since the braid of critical values is (exactly like the saddle point braid) the trivial braid on $n-1$ strands.

In general it is not true that the saddle point braid and the braid of critical values are isotopic, but they must always have the same permutation of strands. So if the saddle point braid is the trivial braid on $n-1$ strands, then the braid of critical values is a pure braid. That is, every critical value ends at $t = 2\pi$ in the same position where it starts at $t = 0$. Constructing Π from such a loop of polynomials g_t gives a branch link L_{branch} with $n-1$ components, but not necessarily the unlink.

Braided open books have also been studied by Rudolph [36], who calls the saddle point braid without orientation the "derived bibraid". The name is justified, since the closure of the saddle point braid, as a link in S^3, is transverse to all pages of the open book whose binding is the braid axis of the saddle point braid and also transverse to all pages of the given braided open book. We may therefore choose orientations for the components of the derived bibraid that turn it into a braid (namely, the saddle point braid) relative to its braid axis and another (in general different) choice of orientation turns it into a generalized braid relative to the fibered link L. Singularity theorists might also be interested in Rudolph's calculation of the Milnor number of a fibered link that is the binding of a braided open book in S^3 in terms of properties of the derived bibraid [36].

The Morse–Novikov number $\mathcal{MN}(L)$ of a link L is a natural number that measures how far a given link is from being fibered. In particular, $\mathcal{MN}(L) = 0$ if and only if L is fibered. In [15] we proved the upper bound $\mathcal{MN}(L) \leq \beta(B)$ for all links L and all braids B that close to L. We use the discussion above to improve this bound.

The Morse–Novikov number $\mathcal{MN}(L)$ is defined to be the minimal number of critical points of any circle-valued Morse map on $S^3\backslash L$ that displays the usual behavior of an open book in a tubular neighborhood of L, that is, locally it is given by $\phi : S^1 \times (D\backslash\{0\}) \to S^1$, $\phi(x, z) = \arg(z)$. We will refer to any such map ϕ as a pseudo-fibration. Upper and lower bounds of the Morse–Novikov number in terms of other link invariants have been found in [25], [37] and [33], but we are not aware of any explicit formula or algorithm that computes it.

Corollary 2.3 *Let B be a braid on n strands whose closure is the link L. Then $\mathcal{MN}(L) \leq \min_{\mathcal{T}} \beta_{\mathcal{T}}(B)$, where the minimum is taken over all embedded trees $\mathcal{T}$ with n vertices.*

Proof From Proposition 2.2 we have for every embedded tree $\mathcal{T}$ with n vertices a loop g_t in $\widehat{X}_n$ whose roots form B and with exactly $\beta_{\mathcal{T}}(B)$ critical points of $\arg(g)$. As in [16] we can construct from a Morse function φ on $S^3\backslash L$, where L is the closure of B with the same number of critical points as follows. By the usual approximation arguments we can assume that the coefficients of g_t are trigonometric polynomials, i.e., polynomials in e^{it} and e^{-it}. Now take this polynomial expression $\lambda^n g_t(\lambda^{-1}u)$, with $\lambda \in \mathbb{R}$ a parameter and $n := \deg_u g_t$, and substitute every e^{it} by another complex variable v and every instance of e^{-it} by the complex conjugate $\bar{v}$. We call the resulting semiholomorphic polynomial f. By construction it is $f|_{v=e^{it}} = g_t$. It was shown in [16] that for sufficiently small values of λ we have that $V_f \pitchfork S^3$ is the closure L of B and $\varphi := \arg(f)|_{S^3\backslash L}$ has the same number of critical points as g. (The polynomial f does not necessarily have a (weakly) isolated singularity at the origin and the intersection $S^3_\rho \cap V_f$ might be different from L for small radii ρ.) Thus φ satisfies the desired property on a tubular neighborhood of L and we have $\mathcal{MN}(L) \leq \beta_{\mathcal{T}}(B)$. Since this holds for any embedded tree $\mathcal{T}$, the result follows. □

Note that $\beta_{\mathcal{T}}(B)$ only depends on the set of $\mathcal{T}$-generators, not on the embedded tree $\mathcal{T}$ per se. Thus the expression $\min_{\mathcal{T}} \beta_{\mathcal{T}}(B)$ refers to the minimum of a finite set of numbers.

Example 2.4 Consider again the example from Fig. 1c. We already know that it is $\mathcal{T}_1$-homogeneous for the embedded tree $\mathcal{T}_1$ in Fig. 1a. Therefore, $\beta_{\mathcal{T}_1}(B) = 0$ and $\mathcal{MN}(L) = 0$. However, expressing the same braid in Artin generators gives $\sigma_2^{-1}\sigma_4\sigma_2^{-1}\sigma_3^{-1}\sigma_1\sigma_2^{-1}\sigma_1^{-1}\sigma_2^{-1}\sigma_4\sigma_3^{-1}\sigma_1\sigma_2^{-1}\sigma_1^{-1}$. We now calculate $\beta_{\mathcal{T}_2}(B) = \beta(B)$ for the line graph $\mathcal{T}_2$. Every generator appears with a positive sign or a negative sign, so the last sum in Eq. (6) does not contribute. Furthermore, the generators σ_2, σ_3 and σ_4 all come with a fixed sign. All instances of σ_2 and σ_3 are negative, while all instances of σ_4 are positive. So these strands do not contribute to the count in $\beta_{\mathcal{T}_2}(B)$. However, the sequence of signs of σ_1 as we traverse the braid word reads $\{+, -, +, -\}$. So there are three sign changes plus one, since the first entry of this list is different from the last one. Thus the bound from [15] would have given $\mathcal{MN}(L) = 0 \leq 4 = \beta(B)$, while our new improved bound in Corollary 2.3 gives

$$0 \leq \mathcal{MN}(L) \leq \min_{\mathcal{T}} \beta_{\mathcal{T}}(B) \leq \beta_{\mathcal{T}_1}(B) = 0 \tag{8}$$

and so $\mathscr{MN}(L) = \min_{\mathscr{T}} \beta_{\mathscr{T}}(B) = 0$.

Proof of Theorem 1.2 Consider a parametrization of the braid B', say

$$\bigcup_{t\in[0,2\pi]} \bigcup_{j=1}^{n-1} (c_j(t), t) \subset \mathbb{C} \times [0, 2\pi], \tag{9}$$

with appropriate functions $c_j : [0, 2\pi] \to \mathbb{C}$. Then $h_t(u) := n \int_0^u \prod_{j=1}^{n-1}(w - c_j(t))\mathrm{d}w$ is a loop in the space of monic polynomials of degree n whose critical points form the braid B' in exactly the given parametrization. After a small deformation of h_t we may assume that its roots are also distinct. The fact that its critical points form B' does not change with this small deformation.

Since the roots of h_t are distinct for all $t \in [0, 2\pi]$, they form a braid on n strands. However, at this stage we do not know what this braid is. We will call it A. Now apply the construction outlined in the proof to Proposition 2.2 to the braid $A' := A^{-1}B$ and basepoint $g_0 := h_0$ to obtain a loop g_t in $\widehat{X}_n$ whose roots form the braid A' and whose saddle point braid is the trivial braid e on $n-1$ strands. Then the composition of h_t and g_t is a loop in $\widehat{X}_n$ whose roots form the braid $AA' = B$ and whose critical points form the braid $B'e = B'$.

3 Singularities of semiholomorphic polynomials

Theorem 1.1 concerns the realization of link types as the link of a weakly isolated singularity of a semiholomorphic polynomial f while at the same time prescribing the link of the singularity of f_u. This type of topological flexibility of the "jet" (in the sense of the literature on the h-principle [21]) of f (while maintaining the link type L) may appear like a typical feature of real algebraic geometry. However, we will see in an example that this flexibility concerning the link of f_u already appears in the complex setting, which is otherwise known to be very rigid.

First we recall some basic definitions concerning the Newton boundary of a mixed polynomial map $f : \mathbb{C}^2 \to \mathbb{C}$ as described in [32]. We may write f as $f(u, v) = \sum_{i,j,k,\ell\geq 0} c_{i,j,k,\ell} u^i \bar{u}^j v^k \bar{v}^\ell$ with all but finitely many coefficients $c_{i,j,k,\ell}$ equal to zero. The support of f, denoted by $supp(f)$, consists of all integer lattice points $(\mu, \nu) \in \mathbb{Z}^2$ such that there are non-negative integers $\mu_1, \mu_2, \nu_1, \nu_2$ with $\mu = \mu_1 + \mu_2$, $\nu = \nu_1 + \nu_2$ and $c_{\mu_1,\mu_2,\nu_1,\nu_2} \neq 0$.

The Newton polygon of f is the convex hull of $supp(f) + (\mathbb{R}^+)^2$. Its boundary consists of a number of vertices and edges. The union of the vertices and compact edges is called the Newton boundary Γ_f of f. There are several properties of Γ_f that can be used to determine if f has a (weakly) isolated singularity, such as convenience and Newton non-degeneracy [32] as well as inner non-degeneracy [2] or partial non-degeneracy [17]. In the case of convenience and Newton non-degeneracy, and inner non-degeneracy it is known that the link of the singularity only depends on the terms of f whose corresponding integer lattice points lie on Γ_f. The sum of these terms is called the principal part of f. In other words, adding terms above the Newton boundary does not change the fact that we have a (weakly) isolated singularity and it does not affect the link type. For more details on the Newton boundary of mixed polynomials we point the reader to [2,17,32].

Example 3.1 Consider the well-known example of $f(u,v) = u^p - v^q$ with $p, q \in \mathbb{N}$ with $p, q > 1$, with an isolated singularity at the origin and the (p,q)-torus link $T_{p,q}$ as the link of the singularity. Since f is holomorphic, we may also study f_u and f_v with regards to their singularities. However, it is easily seen that neither f_u nor f_v has a weakly isolated singularity at the origin.

Instead we may consider $F(u,v) = f(u,v) - uv^k + vu^\ell$ with $k, \ell \in \mathbb{N}$ with $k \geq q$ and $\ell \geq p$. First of all, since both added terms lie above the Newton boundary of f and f is convenient and Newton non-degenerate, it follows that F has an isolated singularity at the origin, whose link is again the (p,q)-torus link $T_{p,q}$. But now we have $F_u(u,v) = pu^{p-1} + v^k$, which has an isolated singularity with link $T_{(p-1,k)}$, and $F_v(u,v) = u^\ell - qv^{q-1}$, which has an isolated singularity with link $T_{(\ell,q-1)}$. We thus have a lot of freedom for the links of F_u and F_v without changing the link of F.

This illustrates that the links of singularities of F_u are not topological invariants of the links of singularities of F. There are different equivalence relations on polynomial map germs with (weakly) isolated singularities related to topological properties (R-equivalence, A-equivalence, V-equivalence, etc.). For example, we might say that two polynomials f_1 and f_2 are A-equivalent if there is a homeomorphism (or diffeomorphism) $h_1 : (B^4_\varepsilon, 0) \to (B^4_\varepsilon, 0)$ and $h_2 : (B^2_\varepsilon, 0) \to (B^2_\varepsilon, 0)$ of the 4-ball and 2-ball of radius ε, respectively, such that on B^4_ε we have $f_2 = h_2 \circ f_1 \circ h_1$, so that in particular the link of f_1 is ambient isotopic to that of f_2. While the link types of the singularities are topological invariants, that is, they do not depend on the representative of the equivalence class of polynomial maps, we cannot expect the same to be true for the link types of f_u. That is, in general we should expect that the link of $(f_1)_u$ is different from that of $(f_2)_u$ even if f_1 and f_2 are in the same equivalence class. After all, even the property of being semiholomorphic itself depends on the particular variables and therefore changes depending on which representative of the equivalence is under consideration. The links of singularities of first derivatives thus may be used to define much finer equivalence relations that treat the polynomial maps as jets. For this note that there is no particular reason to restrict to semiholomorphic polynomial and derivatives with respect to the complex variable. If x_1, x_2, x_3, x_4 are the real coordinates on $\mathbb{R}^4$, we may say that two real polynomial maps $f_1, f_2 : \mathbb{R}^4 \to \mathbb{R}^2$ are link-equivalent as 1-jets if both have (weakly) isolated singularities with ambient isotopic links and $(f_i)_{x_j}$ has a (weakly) isolated singularity for all $i = 1, 2, j = 1, 2, 3, 4$, with the link of $(f_1)_{x_j}$ ambient isotopic to the link of $(f_2)_{x_j}$. We might consider such an equivalence relation up to permutation of links of $(f_1)_{x_j}$ so that a simple permutation of the variables does not change the equivalence class. If a polynomial f is semiholomorphic with $u = x_1 + \mathrm{i}x_2$, then $V_{f_u} = V_{f_{x_1}} = V_{f_{x_2}}$, so that the link types of the real derivatives contain the information about the link of the derivative with respect to u.

We now turn our attention to the proofs of Theorem 1.1 and Theorem 1.5. First, we review some techniques to turn loops g_t of polynomials as in the previous sections into semiholomorphic polynomials with (weakly) isolated singularities.

Since trigonometric polynomials are C^1-dense in the space of 2π-periodic, C^1-functions, we may approximate any loop of polynomials of fixed degree n by a loop g_t whose coefficients are polynomials in $\mathrm{e}^{\mathrm{i}t}$ and $\mathrm{e}^{-\mathrm{i}t}$. Then we may construct a function

$f : \mathbb{C}^2 \to \mathbb{C}$ with a singularity at the origin via

$$f(u, re^{it}) = r^{kn} g_t\left(\frac{u}{r^k}\right), \tag{10}$$

where k is some sufficiently large natural number. The resulting function f is a holomorphic polynomial with respect to u, but is only a polynomial in the variables $v = re^{it}$ and $\bar{v} = re^{-it}$ if g_t (and thus its roots as well) satisfy certain symmetry requirements, namely $g_{t+\pi} = g_t$ or $g_{t+\pi}(u) = -g_t(-u)$, as shown in [14]. If the roots of g_t are distinct, then $\frac{\partial g_t}{\partial u} \neq 0$ whenever g_t is nonzero. Thus $f_u(u_*, v_*) \neq 0$, for all $(u_*, v_*) \in V_f \backslash \{0\}$. By the Cauchy–Riemann equations the real Jacobian matrix of f then has full rank at every $(u_*, v_*) \in V_f \backslash \{0\}$. In other words, if the roots of g_t are distinct, then the singularity at the origin is weakly isolated. With the same techniques as in [7,15] it can be shown that its link is the closure of the braid formed by the roots of g_t. If the roots of g_t form a P-fibered geometric braid, then the singularity is isolated [7,14].

The first author showed in [12] that every link type arises as the link of a weakly isolated singularity of a semiholomorphic polynomial. In [13] it was proved that closures of T-homogeneous braids are real algebraic. Both proofs are constructive and are based on a variation in the idea described above.

In both cases we start with a loop g_t that satisfies the desired symmetry constraints. However, its roots are not distinct for all $t \in [0, 2\pi]$, so that they do not form a geometric braid, but a singular braid with intersection points. Defining f from g_t via Eq. (10) we obtain a semiholomorphic polynomial, whose singularity at the origin is not weakly isolated. By construction f is *radially weighted homogeneous*, that is, its support in $\mathbb{Z}^2$ lies on a straight line of negative slope. In particular, the constructed f is equal to its principal part and is Newton degenerate [17].

We may then find an additional term $A(v, \bar{v})$ such that $f + A$ has a (weakly) isolated singularity, whose link is of the desired form, that is, all singular crossings of the singular braids formed by the roots of g_t are resolved in a very controlled way [12].

The important observation in the context of saddle point braids is that adding $A(v, \bar{v})$ does not change the derivative with respect to u, i.e., $f_u = (f + A)_u$.

Proof of Theorem 1.1 The proof is a modification of the construction in [12]. First of all recall that for every link L and every sufficiently large integer n there is a braid on n strands that closes to L. By the same arguments as in [10] we can find for every sufficiently large even integer $n-1$ a braid B on n strands such that the closure of B^2 contains L as a sublink. Here B^2 denotes the square (or double repeat) of the braid B. It follows that for every pair of links L_1 and L_2 and every sufficiently large even n there exist braids B_1 on n strands and B_2 on $n-1$ strands, so that B_1 closes to L_1 and the closure of B_2^2 contains L_2 as a sublink.

By Theorem 1.2 there is a loop of polynomials h_t in $\widehat{X}_n$ such that the roots of h_t form the trivial braid and the saddle point braid of h_t is B_2. Furthermore, after a homotopy of this loop, which does not change the braid types, we may assume that h_0 is a real polynomial, i.e., all of its roots are real numbers. As in [12] we can also construct a loop of polynomials g_t whose roots form a singular braid B_{sing} such that for every singular crossing c there is a choice of crossing sign $\varepsilon_c \in \{\pm 1\}$ that turns B_{sing} into a classical braid that is isotopic to B_1 if each singular crossing c is replaced by a classical crossing of sign ε_c. The loop of

polynomials g_t can be taken to consist of real polynomials, so that all of the roots of g_t are real numbers for all $t \in [0, 2\pi]$ [12]. We may take the basepoint of g_t to be h_0.

Consider now the loop that is formed by the composition of h_t and g_t. We may approximate its coefficients by polynomials in e^{it} and e^{-it}. Call the resulting loop of polynomials G_t. The approximation can be chosen arbitrarily C^1-close and we can interpolate the original coefficient functions, so that the roots of G_t form the singular braid B_{sing} and the corresponding saddle point braid is B_2. Note that the saddle point braid of g_t was the trivial braid, since it is a real polynomial whose n roots have at most multiplicity 2.

Therefore, the roots of the loop G_{2t} form the singular braid B^2_{sing} and its saddle point braid is B^2_2. Furthermore, the loop obviously satisfies the symmetry constraint $G_{2(t+\pi)} = G_{2t}$, so that f defined from G_{2t} as in Eq. (10) is a radially weighted homogeneous semiholomorphic polynomial.

As in [12] we may now find an extra additive term $A(v, \bar{v})$, which gives $f + A$ a weakly isolated singularity at the origin and resolves all singular crossings in a way that guarantees that the resulting link is the closure of B_1, that is, L_1. The only difference to the proof in [12] is that G_{2t} is not a loop of real polynomials. However, recall that all singular crossings of the roots of G_t occur in intervals where G_{2t} is an arbitrarily close approximation of g_t, which is a loop of real polynomials. This is sufficient for the arguments from [12], so that $f + A$ has a weakly isolated singularity whose link is L_1. Furthermore, as observed above, we have $(f + A)_u = f_u$, so that the zeros of $(f + A)_u$ are exactly $\bigcup_{j=1}^n (r^k c_j(t), re^{it}) \subset \mathbb{C}^2$ with $r \geq 0$, $t \in [0, 2\pi]$ and $\bigcup_{j=1}^n (c_j(t), t)$ a parametrization of the saddle point braid of G_{2t}. Since the critical points of G_{2t} are all distinct (they form a braid), this implies that all roots of $(f + A)_u$ except the origin are regular points of $(f + A)_u$. This means that $(f + A)_u$ has a weakly isolated singularity at the origin and its link is the closure of B^2_2, which by construction contains L_2 as a sublink. □

We see from the proof that in general the link of $(f + A)_u$ has extra components besides L_2. This is because by construction, the saddle point braid of G_{2t} is a 2-periodic braid B^2_2. If on the on the other hand L_2 is the closure of a 2-periodic braid B^2_2 on $n - 1$ strands, such that n is at least the braid index of L_1, then the link of the singularity of $(f + A)_u$ is exactly L_2 without any extra components. Take, for example, the figure-eight knot, which is the closure of the 2-periodic braid $(\sigma_1\sigma_2^{-1})^2$ on three strands. So we may take $B_2 = \sigma_1\sigma_2^{-1}$ and B_1 any braid on four strands. Then the construction above gives a semiholomorphic polynomial map $f : \mathbb{C}^2 \to \mathbb{C}$ with a weakly isolated singularity at the origin and the closure of B_1 as the link of the singularity. Furthermore, the derivative f_u also has a weakly isolated singularity at the origin and its link is the figure-eight knot. So in this case the given knot (4_1) is not only a sublink of the link of the singularity but equal to the link of the singularity. No additional components are required.

Proof of Theorem 1.5 The theorem follows almost immediately from the construction in [13], where we start with a loop g_t, whose roots form a P-fibered geometric braid whose closure is the unknot and that satisfies $g_{t+\pi}(u) = -g_t(-u)$. We deform the critical values of g_t, so that there are some values of t for which there is a critical value equal to 0, which means that at that value of t the roots of the deformed g_t are not disjoint and thus form a singular braid as t varies from 0 to 2π. It is proved in [13] that this deformation can be done in such a way that the resulting critical values $v_j(t)$ still satisfy the condition $\frac{\partial \arg(v_j(t))}{\partial t} \neq 0$ for all $j = 1, 2, \ldots, n - 1$ and all values of t with $v_j(t) \neq 0$. Furthermore, we may assume

that the coefficients of the loop of polynomials $\widehat{g}_t$, which is defined to be the endpoint of the lift of the deformation of the loop of critical values, are polynomials in e^{it} and e^{-it}.

By Theorem 1.4 we can do this procedure, starting with a loop g_t whose saddle point braid is the trivial braid on $n-1$ strands. Since the critical values are distinct throughout the deformation, the same is true for the critical points. It follows that the saddle point braid of $\widehat{g}_t$ is also the trivial braid on $n-1$ strands.

We may then construct f from $\widehat{g}$ as in Eq. (10). By [13] there is a polynomial $A(v, \bar{v})$ such that $f + A$ has an isolated singularity at the origin and its link is the closure of the given T-homogeneous braid. Again, adding A does not affect f_u, so that the roots of $(f+A)_u$ are precisely $(r^k c_j(t), re^{it}) \subset \mathbb{C}^2$, where $r \geq 0$, $t \in [0, 2\pi]$ and $\bigcup_{j=1}^{n-1}(c_j(t), t)$ is a parametrization of the saddle point braid of $\widehat{g}_t$, which is the trivial braid on $n-1$ strands. Thus $(f+A)_u$ has a weakly isolated singularity at the origin, whose link is the unlink on $n-1$ components.

Acknowledgements
B.B. is supported by the European Union's Horizon 2020 research and innovation program through the Marie Sklodowska-Curie grant agreement number 101023017. M.H. is supported by Japanese Society for the Promotion of Science JSPS KAKENHI Grant Number JP18K03296. We would like to thank Mark Dennis for fruitful discussions and the referees for helpful comments.

Funding Information
Open Access funding provided thanks to the CRUE-CSIC agreement with Springer Nature.

Data Availability
Data sharing is not applicable to this article as no datasets were generated or analyzed during the current study.

Author details
[1]Instituto de Ciencias Matemáticas (ICMAT), Consejo Superior de Investigaciones Científicas (CSIC), C/ Nicolás Cabrera, 13-15, Campus Cantoblanco, UAM, 28049 Madrid, Spain, [2]Present address:Departamento de Matemática Aplicada a la Ingeniería Industrial, ETSIDI, Universidad Politécnica de Madrid, Rda. de Valencia 3, 28012 Madrid, Spain, [3]Department of Mathematics, Nagoya Institute of Technology, Showa-ku, Nagoya City, Aichi 466-8555, Japan.

Appendix 1 Visualizations of (pseudo)fibrations

There are several characterizations of the set of fibered links in terms of link invariants [24, 31, 39]. However, even if the proof that a certain link is fibered offers a description of the corresponding fiber surface, it is often difficult to visualize how exactly these fibers fill the link complement. For closures of P-fibered braids the whole fibration is in a nice position relative to the unbook in S^3 or if we consider the corresponding braid in $\mathbb{C} \times [0, 2\pi]$, we might say the fibration is in a nice position relative to the height function $(u, t) \mapsto t$ as in [11]. This allows for nice visualizations of the fibrations of complements of closures of P-fibered braids.

We present three different methods to visualize such fibrations. In the case of non-fibered links similar tools may be used to visualize pseudo-fibration maps. Before we describe these visualizations we would like to mention that the structure of a link and surfaces that foliate its complement also appear in various physical systems, so that visualizations of this form are of interest beyond pure mathematics.

Running a constant electric current through a closed wire in the shape of a given knot K induces a magnetic field $B : \mathbb{R}^3 \backslash K \to \mathbb{R}^3$, which can be calculated explicitly (numerically) from the Biot-Savart law. It has a circle-valued magnetostatic potential function $\varphi : \mathbb{R}^3 \backslash K \to S^1$ with $\nabla \varphi = B$. More details can be found in [4]. Under a small assumption on its behavior near the point at infinity the map φ can be completed to a map on $S^3 \backslash K$ with the desired behavior on a tubular neighborhood of K, so that φ has at least

$\mathscr{MN}(K)$ critical points. The critical points of φ are precisely the zeros of the magnetic field B. The pages of an open book thus have a physical interpretation as the level sets of a magnetostatic potential function. Note, however, that both B and φ depend heavily on the geometry of K. Different, but isotopic, embeddings can lead to very different fields and potentials. In particular, it is not known if it is possible to arrange K in $\mathbb{R}^3$ such that the resulting φ has exactly $\mathscr{MN}(K)$ points.

Other interpretations of fibrations appear in the context of liquid crystals, where the knot is a defect line and the fiber surfaces correspond to layers of material along which molecules arrange themselves [22]. In this context, critical points of a map $\varphi : \mathbb{R}^3 \backslash K \to S^1$ correspond to point defects of the liquid crystal configuration.

In singularity theory the fibrations play an important role via Milnor fibrations, given by the argument of a polynomial map with isolated singularity. The visualization of fibrations presented in this section can therefore be interpreted as visualizations of Milnor fibrations on the 3-sphere $S^3_\varepsilon \backslash V_f$, where the link of the singularity is presented as a braid.

Appendix 1.1 Visualizations from explicit functions

Suppose that B is a P-fibered geometric braid realized via the roots of g_t, a loop in $\widehat{X}_n$. If we know the maps g_t and thus $g(u, \mathrm{e}^{\mathrm{i}t}) := g_t(u)$, we can simply plot the level sets of $\arg(g)$ to obtain a nice visualization.

Often we do not know g_t. For example, we know that T-homogeneous braids are P-fibered and therefore have a P-fibered geometric braid in its isotopy class, but do not have an explicit parametrization of this representative and therefore do not have an explicit description of g_t.

However, with methods as in [15,19] we may find a parametrization of a representative of any given braid B in terms of trigonometric polynomials. This leads to a visualization of the corresponding pseudo-fibration. Furthermore, we may use this approach to prove that for some given links L its Morse–Novikov number can be realized by the argument of a polynomial map.

We illustrate this with the example of the knot 5_2, which is the closure of the braid $B = \sigma_1\sigma_2^3\sigma_1\sigma_2^{-1}$ and was discussed in more detail in [19].

As in [15,19] we find a parametrization of the braid B in terms of trigonometric polynomials via

$$\bigcup_{t\in[0,2\pi]} \bigcup_{j=1}^{3} (z_j(t), t) \subset \mathbb{C} \times [0, 2\pi] \tag{11}$$

with

$$\begin{aligned} z_j(t) = &- \cos\left(\frac{2(t+2\pi j)}{3}\right) - \frac{3}{4}\cos\left(\frac{5(t+2\pi j)}{3}\right) \\ &+ \mathrm{i}\left(\sin\left(\frac{4(t+2\pi j)}{3}\right) + \frac{1}{2}\sin\left(\frac{t+2\pi j}{3}\right)\right). \end{aligned}$$

Then the corresponding loop of polynomials is as usual $g_t(u) := \prod_{j=1}^{3}(u - z_j(t))$. Since the knot 5_2 is not fibered, the resulting argument map $\arg(g), g(u, \mathrm{e}^{\mathrm{i}t}) := g_t(u)$, must have critical points. We have $\mathscr{MN}(5_2) = 2$.

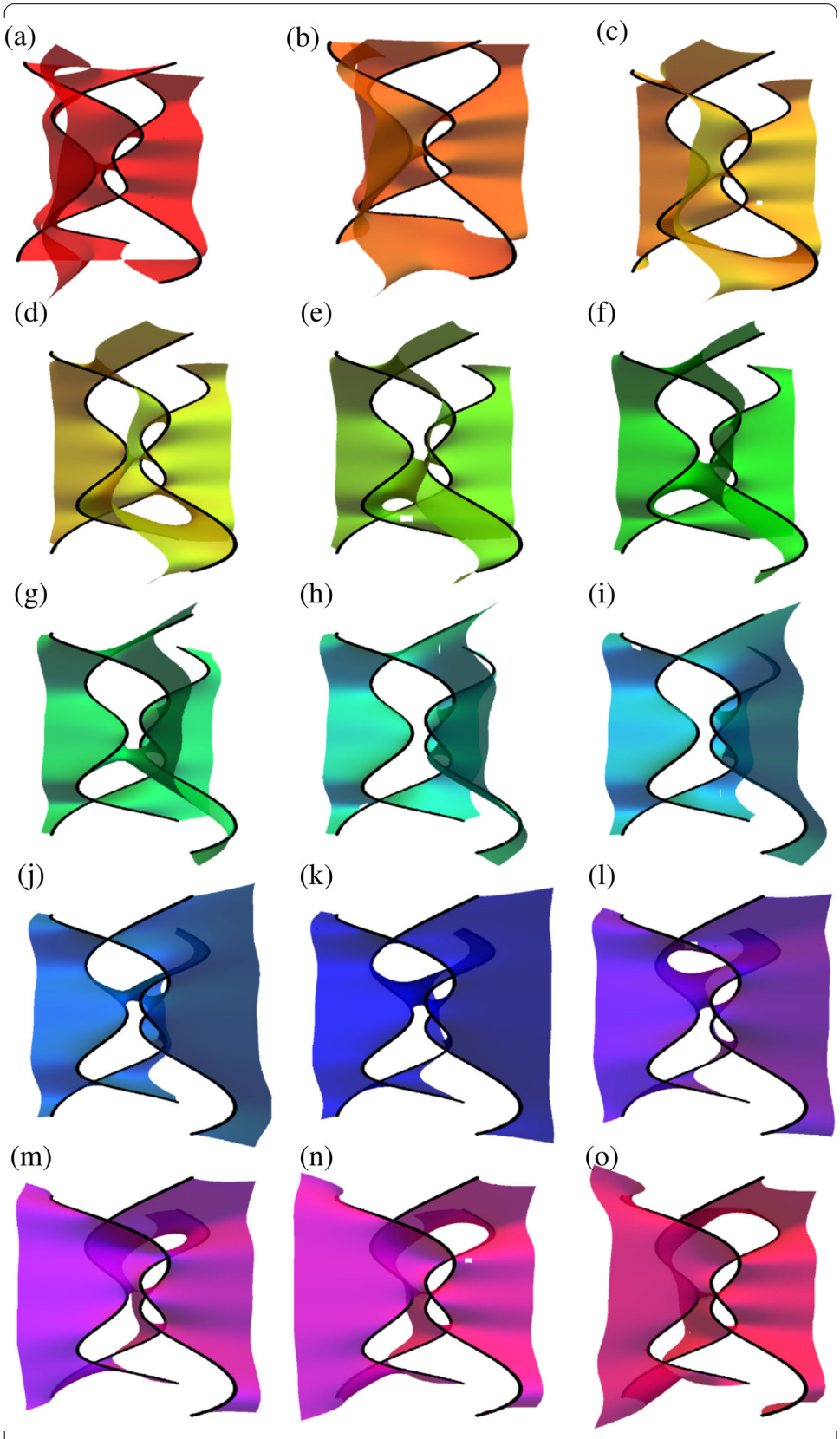

Fig. 6 Level sets $(\arg(g))^{-1}(e^{i\chi})$ of $\arg(g)$. From Subfigs. (**a**)–(**o**) the value χ varies from 0 to $\frac{28}{15}\pi$

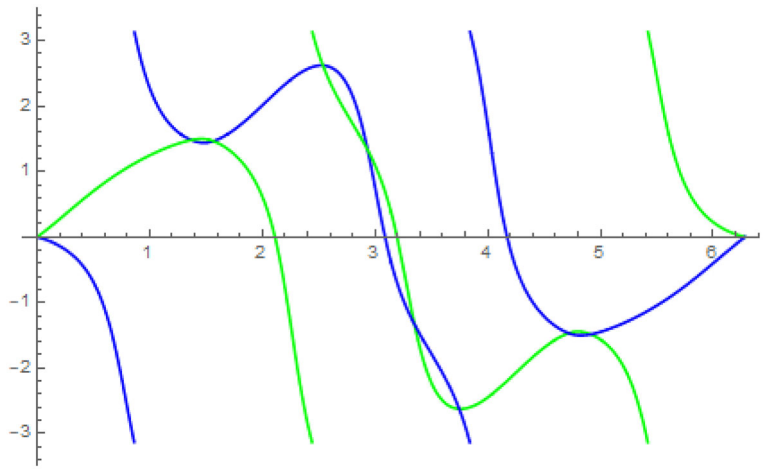

Fig. 7 The graphs of $\arg(v_j(t)), j = 1, 2$, where $v_j(t), j = 1, 2$, are the critical values of g_t

Since we know the function g_t, we can plot level sets of $\arg(g)$, see Fig. 6, and study how the topology changes. All of the subfigures display level sets in $\mathbb{C} \times [0, 2\pi]$, whose common boundary is the braid B. Identifying the bottom and the top plane, results in a solid torus $\mathbb{C} \times S^1$. Its complementary solid torus in S^3 can be filled with meridional disks, so that a visualization of a (pseudo-)fibration in $\mathbb{C} \times [0, 2\pi]$ can be used to visualize the (pseudo-)fibration in S^3.

Some topology changes between surfaces are easier to spot than others. We see, for example, that between the seventh (g) and the eighth (h) subfigure the genus of the surface decreases by one. It then increases between the ninth (i) and tenth (j) subfigure. We can spot another change of topology between the twelfth (l) and thirteenth (m) subfigure.

This superficial visual analysis makes it easy to miss critical points that occur in rapid succession, that is, pairs of critical points $p_1, p_2 \in \mathbb{C} \times [0, 2\pi]$ for which $\arg(g(p_1))$ and $\arg(g(p_2))$ are very close. Going by Fig. 6 we might conclude that $\arg(g)$ has four critical points, since the number of critical points must be even. However, this is not correct.

Figure 7 shows the graphs of $\arg(v_j(t)), j = 1, 2,$, where $v_j(t), j = 1, 2$, are the critical values of g_t. Since critical points of $\arg(g)$ correspond to points with $\frac{\partial \arg(v_j(t))}{\partial t} = 0$, we see immediately from this plot that $\arg(g)$ has exactly 6 critical points. Comparing this with $\mathscr{MN}(5_2)$, we see that it has more critical points than necessary.

As discussed earlier, the critical points of $\arg(g)$ must lie on the saddle point braid, which is plotted in Fig. 8a. In Fig. 8b we have colored the saddle point braid by $\arg(g)$. In this way the critical points are seen as those points where there is a change in the direction with which the color wheel is traversed. Figure 8b also shows a level set of $\arg(g)$. Note that its intersection points with the saddle point braid are its points with horizontal tangent planes.

Knowing the location of the critical points allows us to show the topology changes in the level sets as a critical value is passed. Figure 9 shows such a change that is representative for all changes. Two sheets move toward each other as we approach the critical level set (Fig. 9a). When we reach the level set of the critical value, the two parts meet in a double-cone, whose tip is a critical point of $\arg(g)$ (Fig. 9b). Increasing the value of $\arg(g)$

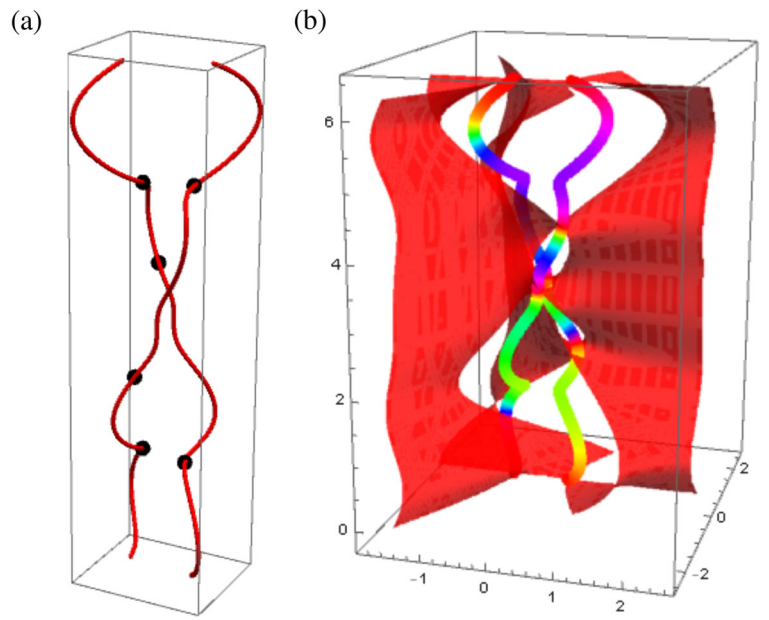

Fig. 8 **a** The saddle point braid and the critical points of arg(g). **b** The saddle point braid colored by arg(g) and a level set of arg(g)

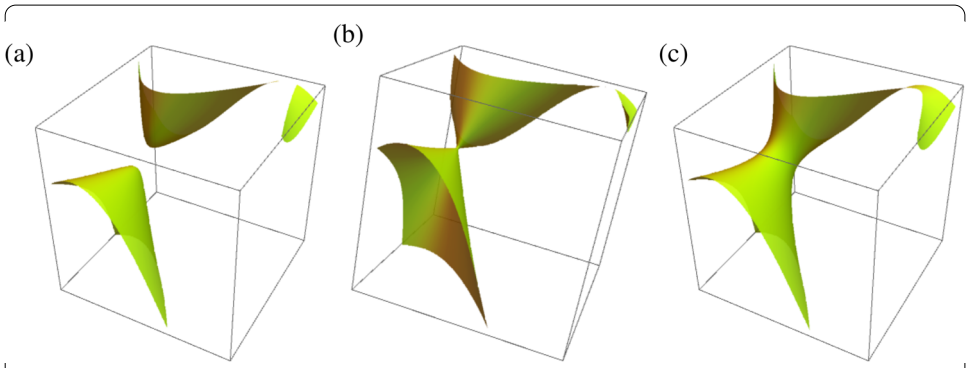

Fig. 9 A local change of topology of a level set of arg(g). Say $\chi \in S^1$ is the critical value of arg(g). **a** Part of $\arg(g)^{-1}(\chi - \varepsilon)$ with $\varepsilon > 0$ and small. **b** Part of the level set $\arg(g)^{-1}(\chi)$. **c** Part of the level set of $\arg(g)^{-1}(\chi + \varepsilon)$ with $\varepsilon > 0$ and small

further results in a level set with a compressing disk (Fig. 9c). The genus has increased by 1. Of course, going through this sequence of pictures in the opposite order, starting with a compressing disk that shrinks to a double cone and splits into two separate sheets, decreases the genus.

We know that the Morse–Novikov number of 5_2 is 2, but arg(g) has 6 critical points. This immediately leads to the question: Could we have chosen a different parametrization of a braid that closes to 5_2 such that the resulting argument map of the polynomial only has two critical points? The answer to this question is "Yes". We will explain why and illustrate with this example a useful technique to prove that a given non-fibered link has Morse–Novikov number equal to 2.

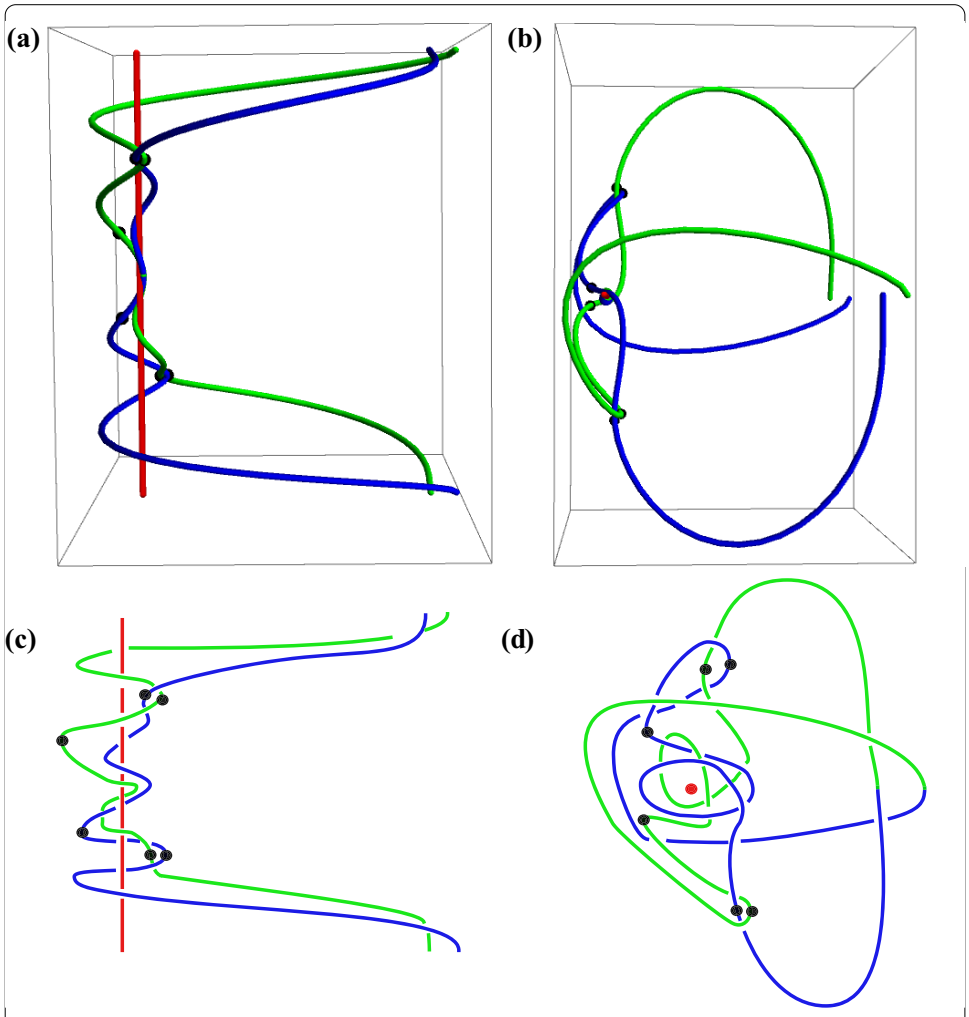

Fig. 10 The braid of critical values $v_j(t)$, $j = 1, 2$, in blue and green, together with the strand $\{0\} \times [0, 2\pi]$ in red. Black points indicate the points where $\frac{\partial \arg(v_j(t))}{\partial t}$ vanishes, corresponding to critical points of $\arg(g)$. **a** The view from the side. **b** The view from the top. **c** A knot diagram obtained from the side view. **d** A knot diagram obtained from the top view

Figure 10 shows the braid that is formed by the critical values of g_t and the strand $\{0\} \times [0, 2\pi]$ both from the side and from the top. Note that the endpoints of the blue strand at the top and bottom match the endpoints of the green strand although the perspective in Fig. 10 makes that difficult to see. The figures also show the six points, where $\frac{\partial \arg(v_j(t))}{\partial t}$ vanishes, corresponding to critical points of $\arg(g)$.

We may deform the braid of critical values in $(\mathbb{C}\backslash\{0\}) \times [0, 2\pi]$ to the braid shown in Fig. 11, which only has two points where the critical values change their orientation. There are two pairs of such points in Fig. 10 that are very close together. In order to go from the braid in Fig. 10 to the one in Fig. 11 we simply have to move the blue and the green strand near these pairs of points. For the lower pair we pull the blue and the green strand from right to left behind the red strand $\{0\} \times [0, 2\pi]$ until the critical point on the blue strand cancels with the next critical point on the blue strand. Likewise, for the upper pair

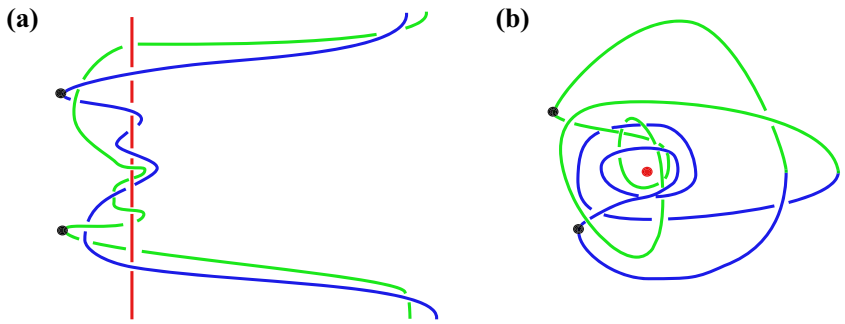

Fig. 11 The deformed braid of critical values. **a** The view from the side. **b** The view from the top

of points we move the blue and the green strand from right to left in front of the red strand. In this case, two critical points on the green strand cancel.

This deformation is a homotopy of the loop $\pi(\theta_n(g_t))$ in V_n, which extends to a homotopy of $\theta_n(g_t)$ in $\widehat{V}_n$. This homotopy lifts to a homotopy of g_t in $\widehat{X}_n$, so that there is a loop of monic polynomials h_t whose critical values form the braid in Fig. 11a, while its roots form the braid B that closes to 5_2. In particular, by construction $\arg(h)$, $h(u, e^{it}) := h_t(u)$, has exactly 2 critical points. Since 5_2 is not fibered, its Morse–Novikov number must be at least 2. We have found a circle-valued Morse map with the required properties and exactly 2 critical points, which shows that $\mathcal{MN}(5_2) = 2$. Of course, we already knew this before, but the method can be applied to any given non-fibered knot or link for which we can deform the braid of critical values in such a way that the number of argument-critical points reduces to 2.

The algorithm in [15] produces for any given link a loop of polynomials g_t. We may then study the corresponding loop of critical values $\pi(\theta_n(g_t))$ and try to deform it in a way that reduces the number of critical points. In general, this produces an upper bound on the Morse–Novikov number. However, if we achieve a deformation whose lift has an endpoint h_t such that $\arg(h)$ does not have any critical points, then obviously the Morse–Novikov number is equal to zero. Likewise, if we already know that the link L in question is not fibered (like 5_2 above), then $\mathcal{MN}(L) \geq 2$. Thus if we achieve a deformation of the critical values such that the corresponding loop of polynomials h_t results in exactly 2 critical points of $\arg(h)$, then the Morse–Novikov number must be equal to 2. If such a deformation does not exist or cannot be found, then we have acquired no new information and are left with the original inequalities $2 \leq \mathcal{MN}(L) \leq m$, where m is the number of critical points of the circle-valued Morse map $\arg(g)$.

Appendix 1.2 Visualizations from Rampichini diagrams and films

As pointed out, the method from the previous subsection requires the knowledge of an explicit function g_t. The problem with this approach is that if we want g_t to have certain properties like inducing a fibration $\arg(g)$, usually (even for T-homogeneous braids) we do not know the loop g_t. We proved its existence in Proposition 2.2, but a key step in this proof was to deform a loop in $\widehat{V}_n$, which lifts to a homotopy of loops in $\widehat{X}_n$ whose endpoint is g_t. This lifting procedure requires solving a 1-parameter family of a set of

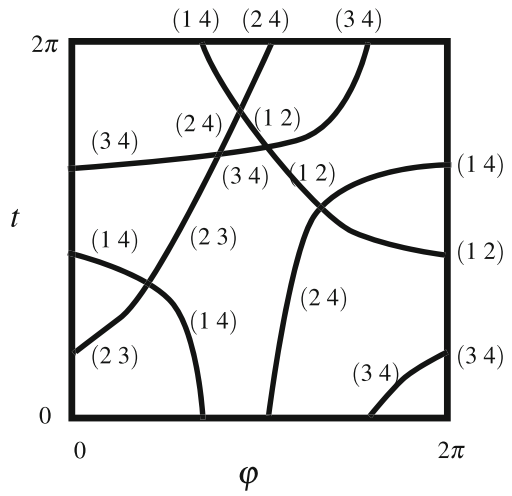

Fig. 12 A Rampichini diagram

polynomial equations, which is challenging even with the help of computers if the degree of the polynomials g_t is $n > 3$.

However, for any braid B and any embedded tree $\mathscr{T}$ we know the loop of critical values in V_n and the basepoint g_0 of a loop g_t such that $\arg(g)$ has exactly $\beta_{\mathscr{T}}(B)$ critical points. This is sufficient to draw the Rampichini diagram of g_t as in [11]. This diagram encodes all the information we need in order to visualize the fibration.

A Rampichini diagram consists of a square that contains a number of curves that are labeled by transpositions. The square should be interpreted as a torus with both the horizontal and vertical edges corresponding to coordinate axis, going from 0 to 2π. The vertical direction corresponds to t, the variable that parametrizes the loop g_t. The horizontal direction corresponds to $\varphi = \arg(g)$.

The curves in the square keep track of the motion of the critical values $v_j(t)$, $j = 1, 2, \ldots, n-1$, of g_t. More precisely, a point with coordinates (φ_*, t_*) lies on a curve if and only if there is a $j \in \{1, 2, \ldots, n-1\}$ such that $\arg(v_j(t_*)) = \varphi_*$.

Since the roots of g_t are assumed to form a P-fibered geometric braid, no curves in the square have horizontal or vertical tangencies. In particular, each curve is strictly monotone increasing (if the corresponding $\frac{\partial \arg(v_j(t))}{\partial t}$ is positive) or strictly monotone decreasing (if the corresponding $\frac{\partial \arg(v_j(t))}{\partial t}$ is negative). We may extend the definition of a Rampichini diagram to loops of polynomials g_t whose roots do not form P-fibered geometric braids, in which case there are points where the curves in the square have vertical tangencies. Assuming a generic non-degeneracy condition, the number of such vertical tangencies is exactly the number of critical points of $\arg(g)$, $g(u, e^{it}) = g_t(u)$. The term "Rampichini diagram" is reserved for loops g_t that correspond to P-fibered braids. If g_t does not correspond to a P-fibered braid, the resulting diagram is simply called a square diagram.

Above we denoted the critical values of g_t by $v_j(t)$. The index j is assumed to be chosen such that the curves $v_j(t) : [0, 2\pi] \to \mathbb{C}$ are smooth. For all values of $t \in [0, 2\pi]$ for which the curves do not intersect each other or the line $\varphi = 2\pi$, there is another (in general different) order. We write $v(t)_j$, $j = 1, 2, \ldots, n-1$, for this second ordering of critical

values, which orders the critical values at a fixed value of t (outside the finite number of forbidden values mentioned above) by their argument between 0 and 2π. In other words, $0 < \arg(v(t)_j) < \arg(v(t)_k) < 2\pi$ if and only if $j < k$. Note that the index coming from this second type of order is not constant along the smooth curves $c_j(t)$. It changes at crossings in the square diagram and when a curve crosses the line $\varphi = 2\pi$. This is also explained in [13]. Since every point on a curve in the square corresponds to a critical value $v(t)_j$, it comes with a transposition τ_j defined from the singular foliation induced by $\arg(g_t)$. These transpositions label the points on the curves in the square. The labels (and thus also the cactus) only change at the line $\varphi = 2\pi$ and at intersection points of the curves, corresponding to a critical value $v(t)$ crossing the line $\varphi = 0$ or two critical values having the same argument, respectively. Therefore, it is sufficient to label the arcs of the curves between such points. This means that for any fixed value of t the labels in the square diagram at that fixed height t, read from left to right, are exactly the cactus of g_t. An example of a Rampichini diagram is displayed in Fig. 12.

For each $t \in [0, 2\pi]$ for which the critical values have distinct arguments the map $\arg(g_t)$ induces a singular foliation on $\mathbb{C}$, similar to [26]. As mentioned in Section 2, the roots of g_t are elliptic singularities and the critical points are hyperbolic points. The Rampichini diagram essentially stores for every value of $t \in [0, 2\pi]$ the information about the cactus of g_t, which is enough to draw the entire singular foliation of $\mathbb{C}$. This combinatorial structure only changes at finitely many values of $t \in [0, 2\pi]$, so that we have a topological description or a visualization of the fibration map $\arg(g)$. All of this is described in more detail in [11,30,34]. This approach to visualize fibrations is quite similar to a very recent visualization of fibrations for homogeneous braids that has been offered by [27].

Figure 13 shows a sequence of singular foliations, while the four roots trace out the braid σ_3. Rampichini calls such a sequence a film [34].

We can see in these figures that the saddle points form a trivial braid on 3 strands. Since the first picture is the same as the last, this sequence of figures represents a loop of polynomials. (The fact that such a loop is realized by polynomials is a consequence of Riemann's existence theorem [11].) We can thus compose loops of this form for any Artin generator and its inverse. In this way, Fig. 13 represents a visual proof of Theorem 1.2.

Figure 14 shows part of a Rampichini diagram that corresponds to the film in Fig. 13. The dotted horizontal lines indicate the heights, that is, the values of t, for which Fig. 13 shows the induced singular foliation. The lowest dotted horizontal line corresponds to the first subfigure in the sequence in Fig. 13 and the highest dotted line corresponds to the last image in the sequence in Fig. 13. As in [13] we only include the transposition labels along an edge of the square and turn the intersections of lines in the square into crossings as in a (virtual) knot diagram with the convention that a line is the undercrossing arc if the corresponding critical value has smaller absolute value at the intersection. With this information and the rules from [11,13] we could reproduce the entire Rampichini diagram with all of its labels.

The cactus of the polynomials corresponding to the first three pictures in Fig. 13 is $\tau_1 = (2\ 3)$, $\tau_2 = (2\ 4)$, $\tau_3 = (1\ 2)$. The fourth figure corresponds to a value of t for which there is a crossing in Fig. 14. Therefore, we have $\arg(v_1) = \arg(v_2)$ and there is no well-defined cactus. The cactus for the fifth figure is $\tau_1 = (2\ 4)$, $\tau_2 = (3\ 4)$, $\tau_3 = (1\ 2)$. The sixth figure has again has no well-defined cactus, since two critical values have the same

argument. The cactus of the seventh figure is $\tau_1 = (2\ 4)$, $\tau_2 = (1\ 2)$, $\tau_3 = (3\ 4)$. The last cactus is equal to the first one.

Starting from any Rampichini diagram we can draw a film as in Fig. 13 that completely describes the fibration.

Rampichini diagrams offer another way to visualize fibrations. Instead of using transpositions to label the curves in the square, we may use band generators, so that $(i\ j)$ is replaced by $a_{i,j}$ if the corresponding line is strictly monotone increasing (or, equivalently, $\frac{\partial \arg(v_k(t))}{\partial t} > 0$ for the corresponding critical value $v_k(t)$) and $(i\ j)$ is replaced by $a_{i,j}^{-1}$ if the line is strictly monotone decreasing (or, equivalently, $\frac{\partial \arg(v_k(t))}{\partial t} < 0$ for the corresponding critical value $v_k(t)$).

We obtain a word in BKL-generators for the fiber surfaces of the fibration as follows. We fix a value $\arg(g) = \varphi_*$, which corresponds to a vertical line in the Rampichini diagram. Reading the BKL-labels of the curves in the Rampichini diagram at intersection points with this vertical line, going from the bottom to the top, spells a BKL-word for the fiber $\arg(g)^{-1}(\varphi_*)$. By varying φ_* we obtain a finite sequence of band words, representing the (topologically equivalent) braided surfaces.

An important aspect of this visualization and the one obtained from a film is the insight that the saddle point braid consists exactly of those points where a fiber surface intersects the corresponding horizontal plane tangentially. Since g_t is holomorphic in u and has distinct roots at each fixed value of t, its critical points $c_j(t)$ are exactly the points where $\frac{\partial \arg(g_t)}{\partial \mathrm{Re}(u)}$ and $\frac{\partial \arg(g_t)}{\partial \mathrm{Im}(u)}$ both vanish. In other words, the gradient vector $\nabla \arg(g_t)(u_*)$ is vertical (and potentially the zero-vector) if and only if $u_* = c_j(t)$ for some $j = 1, 2, \ldots, n-1$. Therefore, $u_* \in \mathbb{C}$ is a critical point of g_t if and only if the intersection of the level set $\arg(g) = \arg(g_t(u_*))$ and $\mathbb{C} \times \{t\}$ at (u_*, t) is tangential.

All of the fiber surfaces are braided surfaces and therefore consist of n disks that are connected by a number of half-twisted bands. Each half-twisted band has exactly one saddle point.

This is a reason why the topological type of the saddle point braid on its own is not that helpful for the visualization. It tells us where the saddle points are, but the crucial piece of information, which of the disks are connected by the corresponding band, is missing. For this we need the additional information of the tree or the cactus of the polynomial, which is stored in the Rampichini diagram.

Appendix 1.3 Fibrations for homogeneous braids

The visualization technique from Section Appendix 1.2 offers a complete graphical description of the fibration without the knowledge of an explicit expression for the fibration map or the loop of polynomials g_t. Furthermore, it illustrates that for T-homogeneous braids the saddle point braid may be chosen to be the trivial braid. However, it requires some extra work to go from a sequence of figures as in Fig. 13 to a sequence of figures as in Fig. 6, which display how the different fiber surfaces sweep out the link complement. In this section, we will describe a new visualization technique for the fibrations of homogeneous braids. As in Section Appendix 1.2 we do not need to know an expression of the corresponding polynomials g_t and the saddle point braid is easily seen to be the trivial braid. Yet we arrive at a graphical description of the fibration in terms of a sequence of fiber surfaces, which makes it perhaps more practical than the technique from Sec-

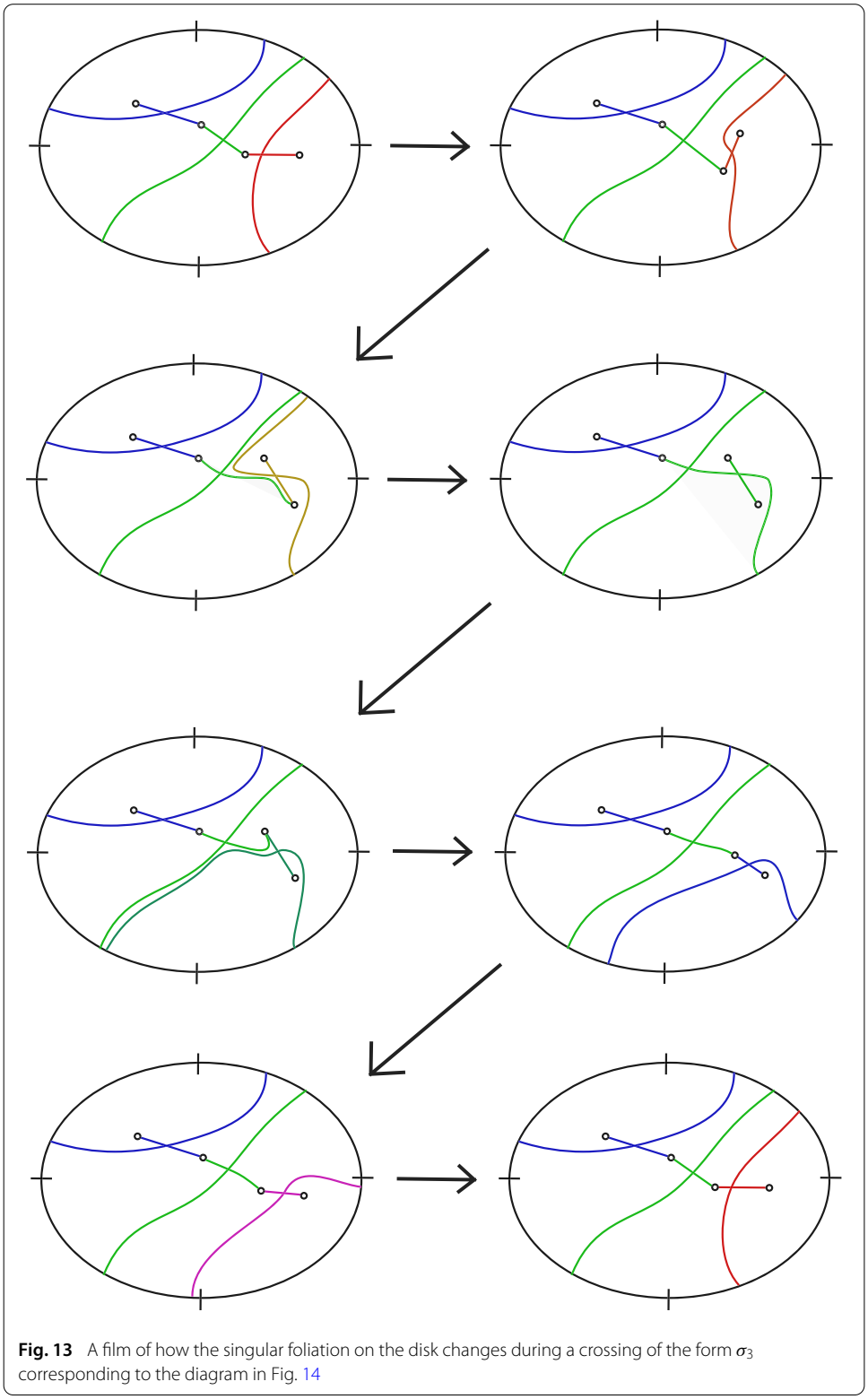

Fig. 13 A film of how the singular foliation on the disk changes during a crossing of the form σ_3 corresponding to the diagram in Fig. 14

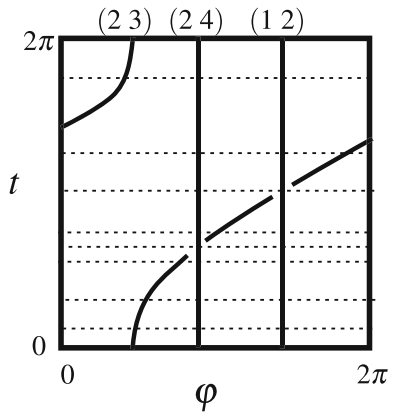

Fig. 14 Part of a Rampichini diagram corresponding to the film in Fig. 13

tion Appendix 1.2. To a certain extent this visualization technique should be adaptable to T-homogeneous braids. At the current stage we content ourselves with the treatment of homogeneous braids.

The rough idea of our technique is displayed in Fig. 15a, which shows a sequence of isotopic surfaces whose common boundary is a link, presented as a closed homogeneous braid. The starting point is a banded surface, whose boundary is the closure of a homogeneous braid on four strands. The fiber surface is thus realized by four disks connected by a number of bands, one for each crossing of the braid. Note that the sign of the crossings within any row does not change, so that the braid is indeed homogeneous. We now push the top disk up until it is located as in the second image in Fig. 15a. The disk is now pointing outwards, that is, having started with a non-zero section of tangent vectors v of the disk, normal to its boundary, pushing the disk as described and moving the tangent vectors with it results exactly in $-v$. Note that now the opposite side of the surface is pointing upwards. In Fig. 15 the two sides of the surface are colored blue and red, respectively. Note such a coloring is possible precisely because all fiber surfaces are orientable.

In order to move from the second image to the third image, we have to push the red disk on the outside down, while moving the blue disk in the layer below it upwards. This is tricky. Later we will describe in more detail how this is done and what happens with the bands between these two disks. For now, the reader will have to accept that there is such a motion of surfaces fixing the boundary that moves the red disk on the outside one layer downwards, while moving the blue disk on the inside one layer up, resulting in the third image. This motion is repeated until we reach the fifth and last image in Fig. 15a, where the red disk on the outside has arrived at the bottom layer.

Each subfigure of Fig. 15a only shows a finite region of S^3. In particular, all surfaces are still compact with identical boundary. In the subfigures after the first one, it might look like there is an additional boundary component originating from the red disk, which in the figure looks like a red annulus. This is in fact not a boundary component of the surface. It is the intersection of the surface with the boundary of the displayed region. Outside of the displayed region the "annulus" is capped off by a disk. These disks grow bigger and bigger while we move the red sheet downwards until it reaches the bottom layer.

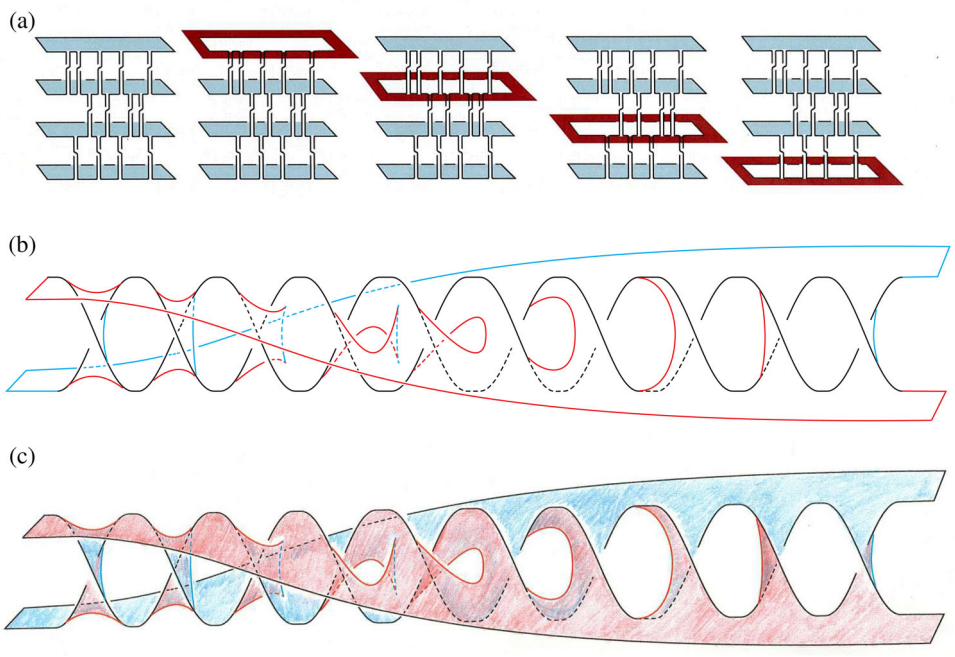

Fig. 15 Fibrations for homogeneous braids. **a** A visualization of several fiber surfaces of a fibration for a homogeneous braid on four strands. **b** An isotopy of a fiber surface that lowers the red outside disk and raises the blue inner disk by one level, highlighting the motion of the contour lines. Going from left to right, we see how a fiber surface is isotoped near a band. **c** The same isotopy, now with a colored shading that indicates the two sides of the surface

We may now pull the red disk on the outside down, while keeping its boundary fixed. It passes through the point at infinity (if we think of our images as placed in $\mathbb{R}^3$) and eventually sits on the inside with its blue side facing up. We have thus reached the first image again. Note that this sequence of surfaces fills the entire link complement, they can be made disjoint and they are isotopies with fixed boundary of the original Seifert surface. Thus if we have a convincing picture for the motion that lowers a red outside disk and raises a blue inside disk one layer, we have a visualization of the fibrations for homogeneous braids. Note that this approach is philosophically similar to Stallings' original proof in [40] that closures of homogeneous braids are fibered. It is built on the fact that surfaces that are obtained from fiber surfaces via an operation called Murasugi sum are themselves fiber surfaces of a fibration. The surfaces for a homogeneous braid are obtained by repeated Murasugi sums of fiber surfaces for braids on two strands. Stallings' proof therefore reduces to the (known) case of braids on two strands. Similarly, our visualization technique is reduced to the particular case of a braid on two strands and the general case of a homogeneous braid is obtained by stacking the pictures as in Fig. 15a.

Figure 15b and c illustrates the motion of the surface that lowers the red outside disk and raises the blue inside disk. It is very important to understand that the displayed surface is not meant to be a fiber surface or part of a fiber surface. Instead, it is a convenient way to visualize the motion of a part of the fiber surface near a band. Starting at the very left of either figure we see a red sheet on top, pointing to the front (outside), and a blue sheet at the bottom pointing into the diagram plane (inside). The two sheets are connected by a

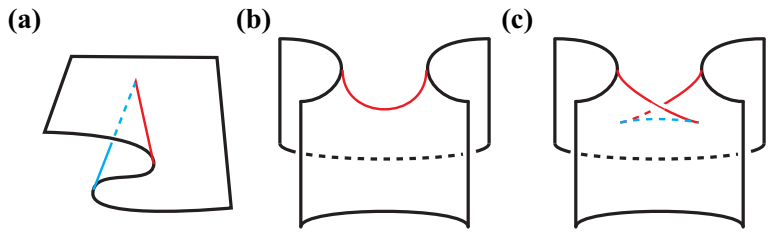

Fig. 16 Folds and cusps. **a** A folded, smooth surface with two contour lines meeting in a point. **b** A saddle point of a surface with one contour line. **c** After an isotopy the surface displays two cusps and three contour lines

half-twisted band as usual. The shading in Fig. 15c indicates the two sides of the surface, blue and red. Figure 15b highlights the contours of the surface, that is, the fold lines where there is change of which side of the surface is facing the reader and thus a change of color. Note that all surfaces are smooth. The contours are an attribute of the chosen perspective on the surface.

Going from left to right in Fig. 15b and c we see how the surface is deformed near a band until at the very right we see a blue sheet at the top, pointing to the back (inside), and a red sheet at the bottom pointing to the front (outside), again connected by a half-twisted band. Therefore, the left end of the figures shows a part of the surface at the beginning of the motion and the right end of the figure shows the desired endpoint of the motion. We now describe the intermediate steps in more detail.

In order to do this, it is helpful to remember some basics on projections of surfaces. Figure 16a shows a part of a surface that is folded in way that creates two contour lines, one blue and one red. The two lines meet at a point as illustrated.

Again we want to emphasize that all surfaces are smooth. The intersection point between the two contours is not a singular point of the surface. It depends on the chosen perspective on the surface and might be understood as a feature of the corresponding projection map from the surface to the diagram plane, rather than an artifact of the surface itself. This shows how we can apply an isotopy to a flat piece of a surface, i.e., without cusps or fold lines, to obtain a surface with two fold lines meeting in a point. Naturally, applying the inverse isotopy brings us from Fig. 16a to a flat, smooth piece of surface.

Figure 16b displays the neighborhood of a saddle point of a surface with one red contour line. We may place a finger on the saddle point and push the saddle point and the surface downwards. If our finger is not orthogonal to the diagram plane, the resulting surface displays two cusps as in Fig. 16c. The single red contour line has split into two red lines, each connecting the boundary to a cusp, and a blue contour that is connecting the two cusps. We may think of this as a first Reidemeister move applied to the fold line. Again, the cusps are not singular points of the surface. We thus have an isotopy from Fig. 16b and c and its inverse allows us to cancel two cusps as in Fig. 16c.

We now return to Fig. 15b and c to discuss the motion of the surface. As mentioned before we start at the left end of the figure, where we have two sheets connected by a half-twisted band. It is also displayed on the left of Fig. 17. The top red surface extends out of the diagram plane toward the reader, while the bottom blue surface extends into the diagram plane. There are three fold lines (or contours) and no cusps. Each contour

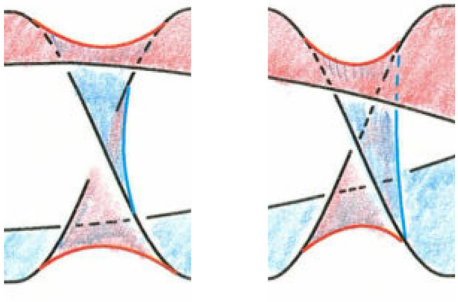

Fig. 17 The initial surface near a crossing and its change after the first step of the isotopy

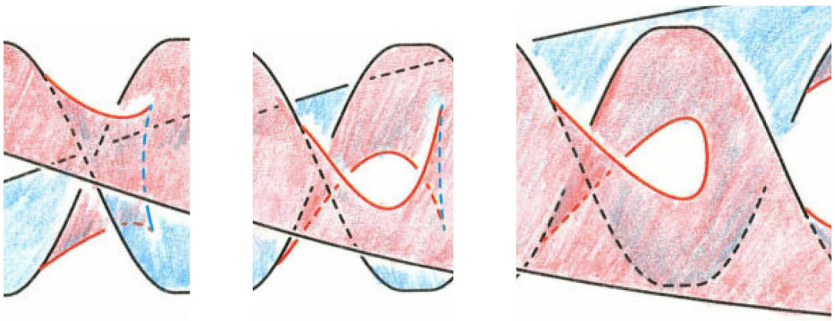

Fig. 18 The surface after the second, third and fourth step of the isotopy near a band

connects two points on the boundary braid. We have two contours at the top and the bottom of the band and one almost vertical contour next to the crossing. Which side of the crossing it is on depends on the sign of the crossing.

Moving our gaze to the right to the next band in Fig. 15c, we see the result of a small isotopy to our original surface in a neighborhood of the same band. It is also shown on the right of Fig. 17. Both at the bottom and the top of the band we may hook a finger around the contour and pull both of them toward the crossing. At the same time the piece of the surface next to the crossing and with the nearly vertical contour is pushed to the right, away from the crossing. Pulling the horizontal contours toward the crossing means that their endpoints on the boundary braid also move toward the crossing. Similarly, pushing the vertical contour away from the crossing makes its two endpoints on the boundary move away from the crossing. Eventually, the endpoints of the horizontal contours have to meet the endpoints of the vertical contour.

Pushing these two intersection points of the contours into the inside of the surface creates two cusps, corresponding to the points where the red (horizontal) and blue (vertical) contours meet, as illustrated with the next band in Fig. 15b and c, also shown on the left of Fig. 18. If we keep pulling the upper horizontal contour down and the lower horizontal contour up, they pass each other as in a second Reidemeister move, see the middle part of Fig. 18 or the fourth band in Fig. 15b and c. We may now apply the isotopy going from Fig. 16b and c, which corresponds to a first Reidemeister move and cancels the two cusps. Note that all of these isotopies of the corresponding surfaces fix the boundary braid. The analogy with Reidemeister moves refers to the motion of the contours, not the boundary

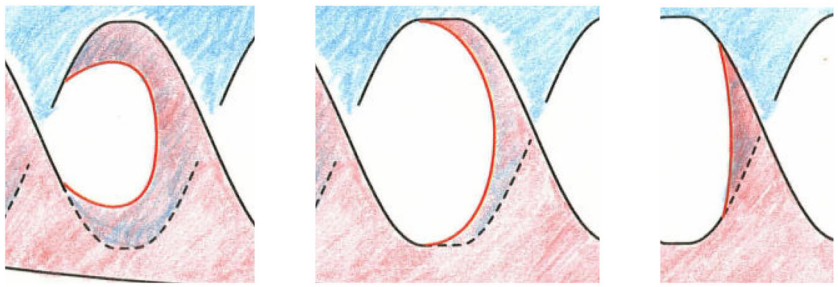

Fig. 19 The surface after the fifth, sixth and seventh step of the isotopy near a band

braid. The resulting surface is shown on the right in Fig. 18, which is the fifth band in Fig. 15b and c. The resulting contour starts a bit above the crossing, goes downwards in front of the crossing, forms a small loop and passes behind the original band back to the boundary braid.

In the next step we grow this loop until it fills the entire gap between the original band and the next band to the right. In doing so, the endpoints of the contour move past the crossing until they lie on the horizontal parts of the boundary braid between two bands, see the left and middle part of Fig. 19.

We may move the contour further toward the band that is directly to the right of the band that we started with until it is a small vertical contour directly to the left of the crossing as seen in the penultimate band in Fig. 15b and c as well as on the right of Fig. 19. Pushing the surface near the crossing toward the right, produces a blue vertical contour directly to the right of the crossing as seen in the last band of Fig. 15b and c. We have described most of this motion of the surface in terms of the motion of the contour lines and the creation and cancellation of cusps. Figure 15c shows how that motion extends to the surface. That is, throughout the motion the red outside disk is pushed downwards and the blue inside disk is pushed upwards, giving us the desired isotopy.

Note that this isotopy moves a band of the original surface to the band directly to the right of it. This is understood as a cyclic operation, that is, the last band is moved to the first band. The fact that all bands are moving to the right is owed to the fact that in the initial surface the blue contours in this example lie to the right of the crossings. If we had pictured crossings with the opposite sign, then the corresponding isotopy would move all bands to the left. This illustrates why this techniques requires that the braid in question is homogeneous. In every row the crossings need to have the same sign, so that there is in every row one direction in which all the bands are pushed.

Our visualization shows a smooth isotopy from a fiber surface to itself, fixing its boundary pointwise throughout and filling the entire space. In order to convince ourselves that this describes a fibration, we have to make sure that all different surfaces can be taken to have pairwise disjoint interiors and that the required behavior on a tubular neighborhood of the link is satisfied.

For a given fibered link and a finite set of isotopic fiber surfaces with pairwise distinct interior, we can always fill the space between the finitely many surfaces with more fiber surfaces, completing the fibration. This can be seen as follows. The union of two Seifert surfaces of the same link with disjoint interiors is the surface of a handlebody. If the two

Seifert surfaces are fiber surfaces, this defines a Heegaard splitting of S^3. The complement of the handlebody surface in S^3 has two connected components, each of which is a solid handlebody. For example, if two fiber surfaces have disjoint interiors and are homeomorphic to some abstract surface Σ, then the solid handlebody is given by $(\Sigma \times I)/\sim$, where I is the interval and $(x, t_1) \sim (x, t_2)$ for all $x \in \partial\Sigma$, $t_1, t_2 \in I$. Since the finite set of fiber surfaces is assumed to have pairwise disjoint interiors, there is a natural ordering of the surfaces as follows. We may pick any of the surfaces as the first surface. Then we draw a meridian around any component of the fibered link and number the surfaces in the order in which the meridian intersects them. Then the second surface has the property that the union of the first and the second surface bounds a solid handlebody that does not contain any of the other finitely many fiber surfaces. The union of the kth and the $(k+1)$st surface bounds a solid handlebody that does not contain any of the other finitely many fiber surfaces and likewise for the union of the last and the first surface. Note that here we rely on the fact that we are indeed dealing with a fibered link and fiber surfaces, so that the union of two surfaces bounds a solid handlebody on either side, i.e, both components of their complement are solid handlebodies. Since the surfaces have pairwise distinct interiors, their interiors all lie completely in one solid handlebody or in the other.

The space $(\Sigma \times I)$ has a natural foliation by surfaces of constant coordinate in the interval I. Since the equivalence relation $\sim$ only affects the boundary, this defines a family of surfaces with disjoint interiors that fill the solid handlebody. The surfaces have a common boundary, which is the fibered link on the handlebody boundary. In particular, there is a smooth family of isotopic Seifert surfaces that fills the solid handlebody whose boundary is the union of the first and the second surface. Continuing in the same manner, we have a natural family of surfaces that fills the handlebody bounded by the kth surface and the $(k+1)$st, while not intersecting the interiors of any of the other displayed surfaces. In this way, we can fill the space between the first and the second surface, between the second surface and the third and so on. Likewise, we can fill the space between the last and the first surface.

In this sense, every finite set of isotopic fiber surfaces with pairwise distinct interiors is a visualization of a fibration. However, if the number of displayed surfaces is too small, it is not particularly useful, since it is difficult to visualize how exactly the space between the two surfaces is filled. In our case, Fig. 15a along with Figs. 17 through 19 shows fiber surfaces and we have explained how to deform one into the next. This deformation pushes the surface (at all points) in the direction of its blue side, that is, in the normal direction that faces away from the blue side, while keeping its boundary fixed. In the abstract picture of $\Sigma \times I$ this simply corresponds to increasing the coordinate in the interval I.

The fact that all the fiber surfaces displayed in our visualization can be taken to have pairwise disjoint interiors can be seen as follows. A key observation is that throughout the isotopy all points on the surface are always pushed in the direction of its blue side. For convenience the sequence of subfigures in Fig. 15a looks like we only move (at most) two disks at a time (red moving down and blue moving up), while the rest of the surface remains stationary. For example, in order to go from the first subfigure to the second we only really move the top disk. Of course, we may push the rest of the surface just a small ε-amount in the direction of its blue side, while we move the top disk, keeping the boundary fixed. We can thus perform the isotopy between the first and the second subfigure in a way that makes the surfaces in the first subfigure and the second subfigure

pairwise disjoint away from their common boundary. Similarly, between the second and third subfigure of Fig. 15a when we move the blue disk upwards, we should not move it all the way to the initial disk in the first subfigure, but instead leave a small ε-amount that the disk can traverse, while the rest of the surface completes the whole isotopy. In this way, all of the surfaces displayed in Fig. 15a can be taken to have pairwise disjoint interiors. In fact, by the same arguments the intermediate surfaces that break down the motion from one subfigure in Fig. 15a to the next and that are indicated in Figs. 17 through 19 can also be taken to have pairwise disjoint interiors. Therefore, all of the displayed surfaces have pairwise disjoint interiors.

We know that all displayed surfaces are fiber surfaces [40], since they are (isotopic to) repeated Murasugi sums of the fiber surfaces of torus links on two strands. Thus it follows from the argument above that the space between the displayed surfaces can be filled with fiber surfaces that have pairwise distinct interiors. The fact that the isotopies between the surfaces are obtained by always pushing in the direction of the blue side, while keeping the boundary fixed also shows that the usual radial behavior that is required for pages of an open book is satisfied in a tubular neighborhood of the link, so that our technique indeed visualizes a fibration.

Figure 15b and c also gives a visual proof of Theorem 1.4 for homogeneous braids. We can now interpret our results and the visualization using the terminology of braided open books in S^3 [11]. Here we think of S^3 as an oriented submanifold of $\mathbb{R}^4$, determined by the volume form ω, $\omega(X_1, X_2, X_3) := \omega_{std}(N, X_1, X_2, X_3)$ for all vector fields X_1, X_2, X_3 on S^3, where $\omega_{std} = \mathrm{d}x_1 \wedge \mathrm{d}x_2 \wedge \mathrm{d}x_3 \wedge \mathrm{d}x_4$ is the standard volume form on $\mathbb{R}^4$ with global coordinates x_1, x_2, x_3, x_4 and $N := \sum_{i=1}^{4} x_i \partial_{x_i}$ is the normal vector of S^3. Every open book in S^3 is described by a fibered link L in S^3 and a fibration map $\Phi : S^3 \backslash L \to S^1$. The fibration allows us to define a natural orientation on each fiber $F_\varphi := \Phi^{-1}(\varphi)$. Pick a point $x \in F_\varphi$. Then we have local coordinates X, Y on a neighborhood of x in F_φ, so that $(\partial_\varphi, \partial_X, \partial_Y)$ is a right-handed basis of tangent vectors on a neighborhood of x in S^3 with respect to the standard volume form on S^3. Equivalently to ∂_φ we can use $-\nabla\Phi$. Since S^3 and all F_φs are orientable manifolds, this determines an orientation on each F_φ. These orientations are consistent with each other in the sense that they induce the same orientation on the common boundary $L = \partial F_\varphi$. We may thus think of a fibered link as an oriented link with its orientation induced by the fibers. If we want to change the orientation of a fibered link on all of its components, we have to compose the fibration map Φ with complex conjugation, mapping φ to $-\varphi$, which reverses the orientations on all fibers.

The unknot O is a fibered knot in S^3, where the fibers of the corresponding fibration map are disks, commonly referred to as *fiber disks*. Since the monodromy map of the fibration, which determines how the disk $F_{2\pi}$ is glued to F_0, is the identity map, the complement of the unknot in S^3 is diffeomorphic to the interior of a disk times S^1. The interior of a disk is naturally diffeomorphic to the complex plane. We may thus represent $S^3 \backslash O$ as $\mathbb{C} \times [0, 2\pi]$ with the complex planes thought of as horizontal planes and the interval as a vertical direction with top and bottom identified. This is of course exactly the ambient space that geometric braids live in. Using t as the variable in $[0, 2\pi]$, the tangent vector ∂_t points vertically upwards, so that the induced orientation of the unknot is the common counterclockwise orientation of the boundary of a disk.

In the introduction we specified that a geometric braid B should be *positively transverse* to the horizontal planes $\mathbb{C} \times \{t\}$, that is, if we think of B as an oriented closed braid in

$\mathbb{C} \times S^1$, then its tangent vector should always have a positive coefficient in front of ∂_t. Note that if B is a P-fibered geometric braid, then the orientation on B that is induced by the corresponding polynomial fibration map $\arg(g_t)$ is exactly of this form.

The concept of a braid and a braid axis can then be generalized as follows. Let (L_1, Φ_1) be an open book on S^3 with fibers $F_{\varphi_1} := \Phi_1^{-1}(\varphi_1)$. As above there is a coordinate atlas of S^3 such that each local coordinate chart has coordinates of the form (φ_1, X, Y), where X and Y are coordinates on a fiber surface F_{φ_1} and φ_1 determines which fiber we are on. Let $L_2 \subset S^3 \backslash L_1$ be an oriented link in S^3. Then we say that L_2 is *positively transverse* to the fibers F_{φ_1} if its tangent vectors (that are consistent with its orientation) always have a positive coefficient in front of ∂_{φ_1}. Suppose now that L_2 is also a fibered link in S^3. So it is the binding of an open book (L_2, Φ_2) with its orientation induced by the orientation of the fibers of Φ_2. Then we say that L_1 and L_2 are *mutually braided* if L_1 (with its orientation coming from the fibers of Φ_1) is positively transverse to the fibers of Φ_2 and L_2 is positively transverse to the fibers of Φ_1. It was shown that this mutual braiding is another equivalent definition of what it means for an open book in S^3 to be braided, that is, a fibered link L is the closure of a P-fibered braid if and only if there is an unknot $O \subset S^3 \backslash L$ such that L and O are mutually braided [11].

Since homogeneous braids are P-fibered, this brings us back to our discussion of saddle point braids. The saddle point braid of a braided open book may then be defined without referring to a loop of polynomials g_t. It is given by the points of tangential intersections between the fiber surfaces of B and the fiber disks of O. In Fig. 15a the fiber disks are vertical, so that the saddle points are the points where the tangent plane of the fiber surface is spanned by the vertical direction and the normal to the diagram plane. We can see from Fig. 15c that throughout the isotopy the saddle points are moving horizontally to the right. Again, if the sign of the crossing had been different, the saddle points would move to the left. It follows that the saddle points form a split unlink on $n-1$ components, where n is the number of strands of the homogeneous braid B. Furthermore, we may choose an orientation for this unlink so that it becomes the trivial braid on $n-1$ strands relative to the same braid axis O.

A comment on this issue of orientation is in order. Since all the surfaces are oriented, the components of the derived bibraid, i.e. the unoriented link that is formed by the saddle points, split into two families, *pos* and *neg*, see [36]. Each saddle point p is a tangential intersection point between a fiber surface and a fiber disk of O. Its component is in *pos* if the orientations of the fiber surface and the fiber disk match at p. It lies in *neg* if the two orientations do not match. Note that for homogeneous braids, this corresponds precisely to the sign of the corresponding band. Saddle points in rows with positive crossings lie on components in *pos* and saddle points in rows with negative crossings lie in *neg*. Note that what we call "*pos*" here is denoted "pos_0" by Rudolph [36]. It is a proper subset of Rudolph's "*pos*".

There are two natural orientations for the derived bibraid. In earlier sections, when we discussed the saddle point braid in terms of loops of polynomials g_t, we naturally parametrized the components of the link consisting of saddle points by the variable t, which parametrizes the loop g_t. Note that different values of $t \in S^1$ correspond to different fiber disks whose boundary is the braid axis O. In other words, we automatically picked an orientation for the derived bibraid that turned it into a braid relative to O, so that it is positively transverse to the fiber disks with boundary O.

In this subsection, we studied the motion of the saddle points as we vary the fiber surfaces (as opposed to varying the fiber disks). We can interpret this as parametrizing the derived bibraid by the variable $\varphi \in S^1$ that parametrizes the family of fiber surfaces. With the induced orientation the derived bibraid is positively transverse to the fiber surfaces, but in general it is not positively transverse to the fiber disks with boundary O. Therefore, with this induced orientation the derived bibraid is not a braid relative to O. Flipping the orientation of the components in *neg* rectifies this and turns the derived bibraid into a braid with braid axis O, the saddle point braid.

Received: 25 August 2023 Accepted: 13 March 2024
Published online: 17 April 2024

References

1. Akbulut, S., King, H.C.: All knots are algebraic. Comm. Math. Helv. **56**, 339–351 (1981)
2. Araújo dos Santos, R.N., Bode, B., Sanchez Quiceno, E. L.: Links of singularities of inner non-degenerate mixed functions. (2022) arXiv:2208.11655
3. Benedetti, R., Shiota, M.: On real algebraic links on S^3. Bolletino dell'Unione Mathematica Italiana. Serie 8 Volume 1B **3**, 585–609 (1998)
4. Binysh, J., Alexander, G.P.: Maxwell's theory of solid angle and the construction of knotted fields. J. Phys. A: Math. Theor. **51**, 385202 (2018)
5. Birman, J.S., Ko, K.H., Lee, S.J.: A new approach to the word and conjugacy problems in the braid groups. Adv. Math. **139**, 322–353 (1998)
6. Bode, B.: Knotted fields and real algebraic links. PhD Thesis. University of Bristol (2018)
7. Bode, B.: Constructing links of isolated singularities of real polynomials $\mathbb{R}^4 \to \mathbb{R}^2$. J. Knot Theory Ramif. **28**(1), 1950009 (2019)
8. Bode, B.: Real algebraic links in S^3 and simple branched covers. Intelligence of Low-Dimensional Topology 2019, RIMS Kokyuroku No. 2129 (2019), 13–28
9. Bode, B.: Real algebraic links in S^3 and braid group actions on the set of n-adic integers. J. Knot Theory Ramif. **29**(6), 2050039 (2020)
10. Bode, B.: Twisting and satellite operations on P-fibered braids. Communications in Analysis and Geometry (In press, 2021)
11. Bode, B.: Braided open book decompositions in S^3. Revista Matemática Iberoamericana **39**(6), 2187–2232 (2023)
12. Bode, B.: All links are semiholomorphic. European Journal of Mathematics **9** (2023), article no. 85
13. Bode, B.: Closures of T-homogeneous braids are real algebraic. Algebraic and Geometric Topology (In press, 2024) arXiv:2211.15394
14. Bode, B.: Links of singularities of inner non-degenerate mixed functions, Part II. arXiv:2307.15340 (2023)
15. Bode, B., Dennis, M.R.: Constructing a polynomial whose nodal set is any prescribed knot or link. Journal of Knot Theory and its Ramifications **28**(1), 1850082 (2019)
16. Bode, B., Dennis, M.R., Foster, D., King, R.P.: Knotted fields and explicit fibrations for lemniscate knots. Proc. R. Soc. A **473**, 20160829 (2017)
17. Bode, B., Sanchez Quiceno, E. L.: Inner and partial non-degeneracy of mixed functions. arXiv:2306.02905 (2023)
18. Brillinger, D.R.: The analyticity of the roots of a polynomial as functions of the coefficients. Math. Mag. **39**(3), 145–147 (1966)
19. Dennis, M.R., Bode, B.: Constructing a polynomial whose nodal set is the three-twist knot 5_2. J. Phys. A: Math. Theor. **50**, 265204 (2017)
20. El Marraki, M., Hanusse, N., Zipperer, J., Zvonkin, A.: Cacti, braids and complex polynomials. Séminair Lotharingien de Combinatoire **37** (1996), B37b, 36p.-B37b, 36p
21. Eliashberg, Y., Mishachev, N.: Introduction to the h-principle. Amer. Math, Soc (2002)
22. Kamien, R.D., Mosna, R.A.: The topology of dislocations in smectic liquid crystals. New J. Phys. **18**, 053012 (2016)
23. Lee, J.M.: Introduction to Smooth Manifolds. Springer, New York (2012)
24. Gabai, D.: Detecting fibred links in S^3. Comment. Math. Helvetici **61**, 519–555 (1986)
25. Hirasawa, M., Rudolph, L.: Constructions of Morse maps for knots and links, and upper bounds on the Morse-Novikov number. arXiv:math/0311134 (2003)
26. Ito, T., Kawamuro, K.: Open book foliations. Geometry & Topology **18**, no. 3 (2014), 1581–1634
27. Miller, M.: Explicitly describing fibered 3-manifolds through families of singularly fibered surfaces. Proc. Sympos. Pure Math. "Frontiers in Geometry and Topology." (In press, 2023) arXiv:2306.13081
28. Milnor, J. W.: Singular points of complex hypersurfaces. Princeton University Press (1968)
29. Montesinos-Amilibia, J.M., Morton, H.R.: Fibred links from closed braids. Proc. Lond. Math. Soc. **62**, 167–201 (1991)
30. Morton, H. R., Rampichini, M.: Mutual braiding and the band presentation of braid groups. Knots in Hellas '98, Proceedings of the International Conference on Knot Theory and its Ramifications, eds. C. Gordon et al. (World Scientific, 2000), 335–346
31. Ni, Y.: Knot Floer homology detects fibred knots. Invent. Math. **170**, 577–608 (2007)
32. Oka, M.: Non-degenerate mixed functions. Kodai Mathematical Journal **33**(1), 1–62 (2010)
33. Pajitnov, A.: On the tunnel number and the Morse-Novikov number of knots. Algebr. Geom. Topol. **10**, 627–635 (2010)
34. Rampichini, M.: Mutually braided links, films and exchangeability. J. Knot Theory Ramif. **10**(5), 739–761 (2001)
35. Rudolph, L.: Some knot theory of complex plane curves. Enseign. Math. **29**, 185–208 (1983)

36. Rudolph, L.: Isolated critical points of mappings from $\mathbb{R}^4$ to $\mathbb{R}^2$ and a natural splitting of the Milnor number of a classical fibred link, Part II, Geometry & Topology: Manifolds, Varieties and Knots, Proceedings of the 1985 Georgia Topology Conference, eds. C. McCrory and T. Shifrin (Marcel Dekker, New York 1986), 251–263
37. Rudolph, L.: Murasugi sums of Morse maps to the circle, Morse-Novikov numbers, and free genus of knots. arXiv:math/0108006 (2001)
38. Salter, N.: Stratified braid groups: monodromy. arXiv:2304.04627 (2023)
39. Stallings, J. R.: On fibering certain 3-manifolds. In: Topology of 3-manifolds and related topics (Proc. The Univ. of Georgia Institute, 1961), ed. M. K. Fort Jr. (1962), 95–100
40. Stallings, J.R.: Constructions of fibred knots and links. In: Algebraic and Geometric Topology Proc. Symp. Pure Math., XXXII, Amer. Math. Soc., Providence (1978), 55–60

Publisher's Note